CZECH TECHNICAL
UNIVERSITY IN PRAGUE

FACULTY OF MECHANICAL
ENGINEERING

MASTER'S
THESIS

2017

ZBYŠEK
RYVOLA

Declaration

I hereby confirm on my honour that I personally prepared the present academic work and carried out myself the activities directly involved with it under the guidance of Ing. Yun Kukchol and Dr.Ir. Nathanael Panagung Tandian M.Sc.. Cited sources of literature are perceptibly marked and listed at the end of this thesis.

In Prague, January 2017 Zbyšek Ryvola

Annotation

Author:	Zbyšek Ryvola
Diploma thesis name:	The Steam Leakage in the Labyrinth Seal
Academic year:	2016/ 2017
Department:	Power engineering
Supervisor:	Ing. Yun Kuk Chol
Consultant:	Dr.Ir. Nathanael Panagung Tandian M.Sc.

Bibliographic data:	Number of pages: 55 Number of figures: 28 Number of tables: 16 Number of appendices: 3
Klíčová slova:	Labyrintová ucpávka, únik páry, CFD, modely úniku páry, porovnání analytických a numerických výsledků úniku páry
Keywords:	Labyrinth seal , mass flow leakage, CFD, existing leakage models, comparison of analytical and numerical mass flow leakage results

Anotace: Tato diplomová práce pojednává o úniku páry labyrintovou ucpávkou. Porovnány byly dva rozdílné způsoby vyhodnocení množství páry protékající labyrintovou ucpávkou. První způsob používá empirické vztahy, které byly odvozeny na zakládě výsledků z experimentálních měření. Druhý způsob používá program ANSYS FLUENT 16.0 pro CFD analýzu proudění. Ke správného vyhodnocení proudění bylo nutné určit dostačující kvalitu sítě a vhodný turbulentní model. Výsledkem této práce bylo ověřit správnost empirických vztahů porovnáním s numerickými výpočty CFD analýzy**.**

Abstract: This thesis contains basic information about mass flow leakage through labyrinth seal. Two different approaches of predicting mass flow rates were compared. The first approach of mass flow rate prediction is using existing leakage models which are empirical formulas based on experimental data. The second approach is to build CFD modelling in numerical simulation software which have been specified as ANSYS FLUENT 16.0 and decide what is the sufficient mesh quality and find the most suitable turbulent model, in order to correctly compute mass flow rates. The result of this paper is to verify the accuracy of the empirical relationships using CFD calculations.

Acknowledgements

This thesis is one of the fulfilments required for finishing Master program. Therefore I would like to thank several people who helped me and supported me during the process of writing this thesis:

1. I would like to express my sincere thanks to my supervisors Ing. Yun Kuk Chol and Dr.Ir. Nathanael Panagung Tandian M.Sc., for their patience, advice and guidance during the process of writing this thesis.

2. I thank my family for their support and encouragement during the entire course of my study.

3. My friends who helped me and who were with me when i needed the most.

1. TABLE OF CONTENT

1 INTRODUCTION 4
2 LABYRINTH SEALS 5
3 REVIEW OF EXISTING LEAKAGE MODELS 8
4 RESEARCH OBJECTIVES 17
5 CALCULATION OF EXISTING LEAKAGE MODELS 18
5.1 Samoylovich equation 19
5.2 Stodola equation 20
5.3 Aungier equation 21
5.4 Kearton equation 22
5.5 Zalf equation 24
6 NUMERICAL CALCULATION 25
6.1 Introduction 25
6.2 Governing equations 26
6.2.1 Turbulent models 27
6.2.1.1 Standard k-ε model 27
6.2.1.2 Shear-Stress Transport (SST) k-ω Model 29
6.2.1.3 Reynolds Stress Model (RSM) 31
6.3 Meshing 33
6.4 Fluent solver settings 35
6.5 Mesh and turbulent model selection 36
7 RESULTS AND DISCUSSION 41
8 CONCLUSION 44
9 REFERENCES 45
10 LIST OF APPENDICES 48

2. TABLE OF FIGURES

Figure 2-1 Principal labyrinth seal Geometric parameters. [3].....5
Figure 2-2 Characteristic flow through a labyrinth seal [3] 6
Figure 2-3 Schematic diagrams illustrating a selection of labyrinth seals. [3] 7
Figure 3-1 The seal contraction ratio [5].....10
Figure 3-2 The seal throttling coefficient [6] 12
Figure 3-3 The throttling coefficient [6].....12
Figure 3-4 The seal carryover coefficient [6] 13
Figure 3-5 Carryover coefficient.....15
Figure 4-1 Design of labyrinth seal.....17
Figure 6-1 Labyrinth seal dimensions 33
Figure 6-2 Mesh density.....33
Figure 6-3 Grid independence analysis of mass flow leakage for high pressure boundary conditions.....36
Figure 6-4 Velocity magnitude of fluid using k-ε model 37
Figure 6-5 Velocity magnitude of fluid using Reynolds stress model 37
Figure 6-6 Velocity magnitude of fluid using SST k-ω model 37
Figure 6-7 Stream function [kg/s] of fluid using k-ε model.....38
Figure 6-8 Stream function [kg/s] of fluid using Reynolds stress model 38
Figure 6-9 Stream function [kg/s] of fluid using SST k-ω model.....39
Figure 7-1 Mass flow rates at high pressure boundary conditions 43
Figure 7-2 Mass flow rates at intermedial pressure boundary conditions.....43
Figure 7-3 Mass flow rates at low pressure boundary conditions.....43
Figure 9-1 Area A, lowest grid resolution i
Figure 9-2 Static pressure of fluid using k-ε model.....ii
Figure 9-3 Static pressure of fluid using Reynolds stress model.....ii
Figure 9-4 Static pressure of fluid using SST k-ω model ii
Figure 9-5 Percentage difference between numerical and analytical data for high pressure boundary conditions vi
Figure 9-6 Percentage difference between numerical and analytical data for intermedial pressure boundary conditions.....vi
Figure 9-7 Percentage difference between numerical and analytical data for low pressure boundary conditions vii

3. LIST OF TABLES

Table 5-1 Given dimensions of labyrinth seal 18
Table 5-2 Summary of existing leakage model results.....24
Table 6-1 Skewness range 34
Table 6-2 Mesh quality parameters.....35
Table 6-3 Summary of Fluent solver setting.....35
Table 6-4 Results of mass flow leakage for High pressure boundary conditions ..36
Table 6-5 Numerical and analytical data of mass flow leakage for high pressure boundary condition.....39
Table 6-6 Deviation between numerical and analytical data for high pressure boundary condition.....40
Table 7-1 Inlet boundary conditions 41
Table 9-1 Number of cell division i
Table 9-2 Mass flow rate results for high pressure boundary conditions..... iii
Table 9-3 Percentage deviation between numerical and analytical data for high pressure boundary conditions iii
Table 9-4 Mass flow rate results for intermedial pressure boundary conditions..... iv
Table 9-5 Percentage deviation between numerical and analytical data for intermedial pressure boundary conditions..... iv
Table 9-6 Mass flow rate results for low pressure boundary conditions v
Table 9-7 Percentage deviation between numerical and analytical data for low pressure boundary condition v

4. NOMENCLATURE

a_0	Initial cell length [mm]
C_c	Carryover coefficient by Eungier [-]
C_R	Contraction ratio by Eungier [-]
C_t	Throttling coefficient by Eungier [-]
D	Distance of each meshed area [mm]
h	Height of teeth [mm]
i	Specific enthalpy [$J \cdot kg^{-1}$]
J	Mass flux [$kg \cdot m^{-2}$]
k_u	Carryover coefficient [-]
l	Pitch [mm]
$\dot{m}$	Mass flow rate through labyrinth seal [$kg \cdot s^{-1}$]
$\dot{m}_{CR}$	Critical mass flow rate through labyrinth seal [$kg \cdot s^{-1}$]
n	Number of seal blades (teeth) [-]
p_1	Seal inlet pressure [Pa]
p_2	Seal outlet pressure [Pa]
q	Scale factor [-]
R	Rotor radius [mm]
R_g	Gas constant [$J \cdot mol^{-1} \cdot K^{-1}$]
R_i	Tip radius of tooth [mm]
R_m	Mean radius of clearance between tooth and stator wall [mm]
R_o	Stator radius [mm]
S	Average flow through [m^2]
T_1	Inlet temperature of steam [K]
T_2	Outlet temperature of steam [K]
t, Δ	Span of the teeth [mm]
u	Fluid velocity [$\boldsymbol{m \cdot s^{-1}}$]
δ	Radial clearance [mm]
v_1	Specific volume of steam at the inlet [$\boldsymbol{m^3 \cdot kg^{-1}}$]
ε	Pressure ratio [-]
ε_{cr}	Critical pressure ratio [-]
ρ_1	Inlet density of steam [$\boldsymbol{kg \cdot m^{-3}}$]
μ	Dynamic viscosity [$\boldsymbol{m^2 \cdot s^{-1}}$]
μ_c	Seal contraction ratio [-]
κ	Poisson's constant [-]

1 INTRODUCTION

In response to increasing demand for higher levels of productivity, turbo machines are designed to operate at high pressure, speeds, temperature fluid flow and operate more efficiently. Consequently sealing of High Speed Turbo- machines to decrease the flow losses has been a major engineering challenge since the inception of steam turbines. Due to various designs and used materials at this time we have many different seals such as lip seals, alternative elastomer and plastic seals, mechanical seals, clearance seals, magnetic fluid seals etc.

Seals are used to introduce the friction in the fluid flow path to reduce the flow leakage and are subdivided into contact and non contact seals. Although contact seals have many advantages from engineering point of view as they fully constrict losses between two or more parts and thus increase the efficiency of the machine effectively as desired. However these seals are not applicable for higher speeds, where friction forces degrade the rubbing parts but also possess excessive heat generation problem. In that case the best option to choose are annular non-contacting seals, which help to create a resistence to fluid flow by extensive generation through tortuous flow paths. To meet the condition of high level of production it resulted in a need to reach optimum balance between turbomachine's leakage characteristics and its rotodynamic performance, while tightening rotor and stator clearances. These seal has proven invaluable influence to their leakage prevention characteristics and their non-contacting nature allowing rotor speeds to be increased. Today we have various annular gas seals as labyrinth seals, pocket dumper seals, hole-pattern and honeycomb seals. The most widely used and simplest are labyrinth seals, that are taken into account in this research. [1], [2]

2 LABYRINTH SEALS

In its simplest form labyrinth seal consist of a series of fins (teeth) and corresponding chambers forming a restriction to the flow and a volume for expansion, as illustrated in Figure 2-1. The clearance between tooth and the stator or rotor wall helps to increase the kinetic energy of the fluid flow by throttling and converting static pressure difference energy to kinetic energy. After each throttle some of the kinetic energy associated with the flow is dissipated by turbulence induced by the intense shear stress and eddy motion in the next chamber, as illustrated in Figure 2-2. The use of a tortuous path between different static pressure regions, incorporating a series of non-contacting restrictions and cavities in the form of labyrinth seal, was implemented by Parson for his steam turbine concept in 1982. Labyrinth seal have proven reliability in wide range of application.

[1], [2], [3]

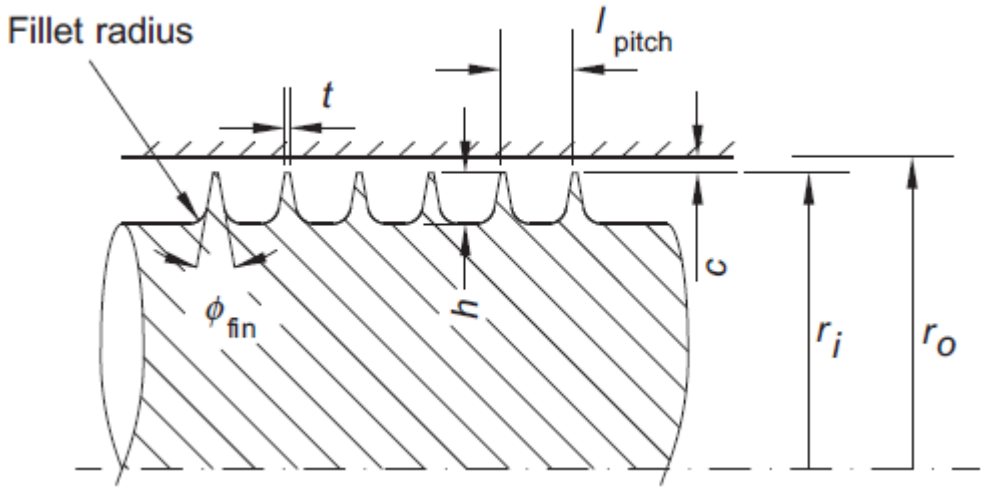

Figure 2-1 Principal labyrinth seal Geometric parameters. [3]

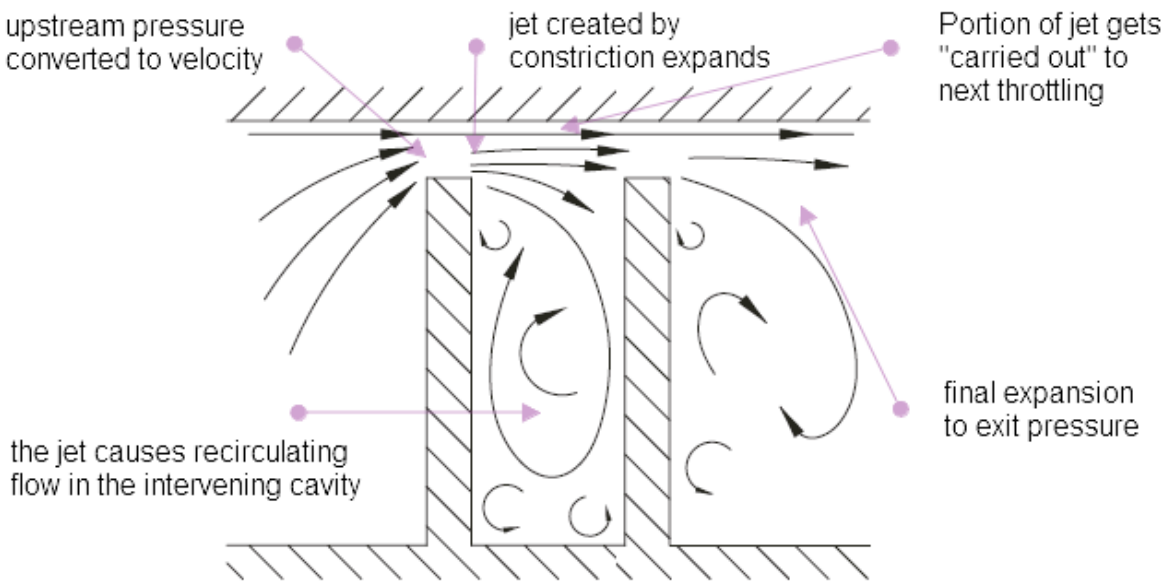

Figure 2-2 Characteristic flow through a labyrinth seal [3]

The principal geometric parameters of typical labyrinth seals can be categorized in axial rotating flow, where the axis of the teeth are coincident with the axis of the shaft, or in radial sealing applications, where the teeth are perpendicular to the shaft axis. The labyrinth seal we can subdivide into straight through, stepped and staggered (see Figure 2-3). The straight through seals we can categorize as teeth on rotor (TOR) or teeth on stator (TOS) in dependence if teeth can rotate or be stationary. In general to improve stability of the system and heat pickup, it is desirable to have teeth on the inner member in the case of axial application. The design of straight through labyrinth seal in practical applications typically involves a compromise between the number of teeth and a pitch that is large enough to provide that the kinetic energy of fluid flow is completely dissipated in the cavity. In terms of modelling various factors (geometry, flow and operating conditions) which constitute the boundary conditions do not operate independently, therefore it needs to be studied to determine the effect of each on the fluid flow leakage. The geometry of the labyrinth seal flow being one of those prominent parameters. Other parameters that affects labyrinth seal performance (leakage) are the fluid flow boundary conditions and the relative movement of the shaft (rpm).

[1], [2], [3]

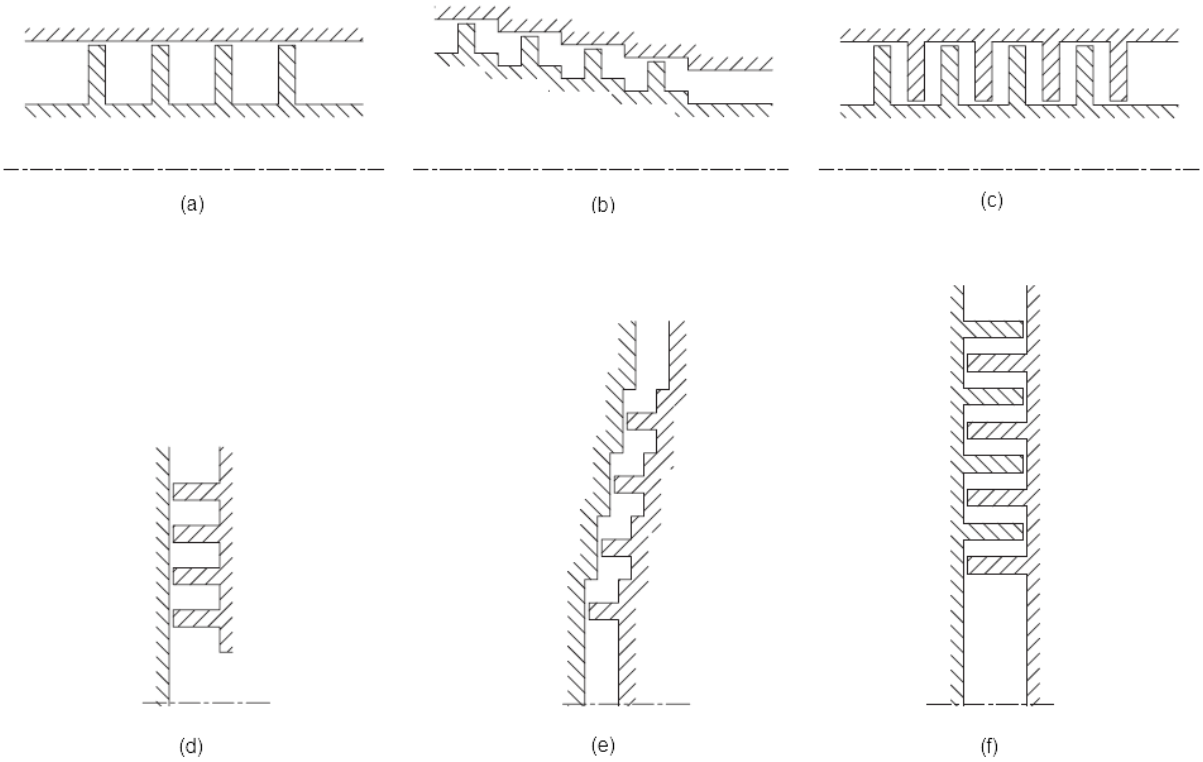

Figure 2-3 Schematic diagrams illustrating a selection of labyrinth seals. [3]

Axial applications: (a) Straight through, (b) stepped and (c) staggered.

Radial applications: (d) Straight through, (e) stepped and (f) staggered.

The increasing demand for energy has fostered the development of more efficient turbo-machinery as turbines are. It resulted in ever-tightening tooth clearances in labyrinth seals. The labyrinths currently in use have the ratio of the order of 1:100. Their undesirable rotor-dynamic characteristics have raised concerns about rotor-dynamic stability of the rotating machinery. The improvement in determining fluid forces damping coefficients for rotor-dynamic calculation of a turbine corresponds with better prediction of fluid leakage, therefore leakage in labyrinth seals has to be determined more accurately. Generally neglected inertia of the fluid in low speed rotor-dynamic calculations can no longer be used due to the inertia of the fluid flow at high RMPs of the shaft. *„This further emphasizes the need of accurate empirical formula for labyrinth seals leakage so as to improve bulk flow models used to better estimate the fluid damping coefficients in the study of rotor dynamics.* [1]

3 REVIEW OF EXISTING LEAKAGE MODELS

One of the first pioneering papers was made by Martin in 1908, in which the first use of „labyrinth packing“ was attributed to Charles A. Parson, who used these seals to reduce leakage of the flow in his steam turbine. Martin considered labyrinth seals as a series of throttling process similar to the flow through a series of orifices. The first equation presented by Martin assumed a linearly varying pressure drop across the seal and isothermal flow. He assumed that the kinetic energy of the fluid entering the cavity was completely dissipated through turbulence and additionally the pressure across each constriction to be very small or treated that the flow always was in subcritical state through the labyrinth seal. He also neglected the effect of kinetic energy carry over and assumed that carry over coefficient is equal to 1. This approach was purely analytical with various false assumptions and he didn't compare his evaluated calculation against any experimental data. This simple equation models the leakage flow rate based on the work done to achieve the required pressure drop have contributed to the fact it that all other authors tried to address the wrong assumptions made by Martin and improved his formula.
[1], [2], [4]

$$\dot{m} = \frac{S \cdot p_1}{\sqrt{R \cdot T_1}} \cdot \sqrt{\frac{1 - \left(\frac{p_2}{p_1}\right)^2}{1 - ln\left(\frac{p_2}{p_1}\right)}} \tag{3-1}$$

In his 1927 book on steam and gas turbines, Stodola considered flow leakage through staggered and radial seals with clearances that can be made as small as 0,2 mm. He analysed compressible flow and provided two separate equations to calculate flow leakage one for subsonic flow and one for chocked flow. He mentioned that for a large number of teeth the mass flow rate is inversely proportional to the square root of the number of teeth. Stodola presented the experimental results on interlocking seals with axial clearances varying from 0,14 mm to 0,38 mm and for pressure ranging from 0,9 bar to 9,8 bar. Stodola assumed that shaft rotation would have little effect on the axial flow rate and thus he performed the tests with non-rotating shaft and completely neglected the effects of shaft rotation on fluid flow leakage. Like Martin, he also assumed that the kinetic energy

gets completely dissipated in the cavity and neglected the effect of kinetic energy carry over. Using Stodola's equations for his test case the values of leakage flow matched the experimental data results with an error of less than 10%.
[1], [2], [4]

Stodola's equation in case that critical speed of flow will not occur in any labyrinth:

$$\dot{m} = \mu_c \cdot S \cdot \sqrt{\frac{{p_1}^2 - {p_2}^2}{p_1 \cdot v_1 \cdot n}} \qquad [kg/s] \tag{3-2}$$

Stodola's equation in case that the critical speed of flow will occur in last labyrinth:

$$\dot{m} = \mu_c \cdot S \cdot \sqrt{\frac{p_1}{v_1 \cdot n}} \qquad [kg/s] \tag{3-3}$$

Seal clearance area:

$$S = 2 \cdot \pi \cdot r_{seal} \cdot \delta \tag{3-4}$$

He additionally developed a graphical method for analysing seals with varying areas and shapes, as illustrated in Figure 3-1, where the shapes are substantially enlarged to increase resolution of the shapes of flow around edges. To predict the tooth shape change we can consider mean value equal to 0,75 (however for this case μ=0,71). The tooth thickness is often around 0,5 mm.
[5]

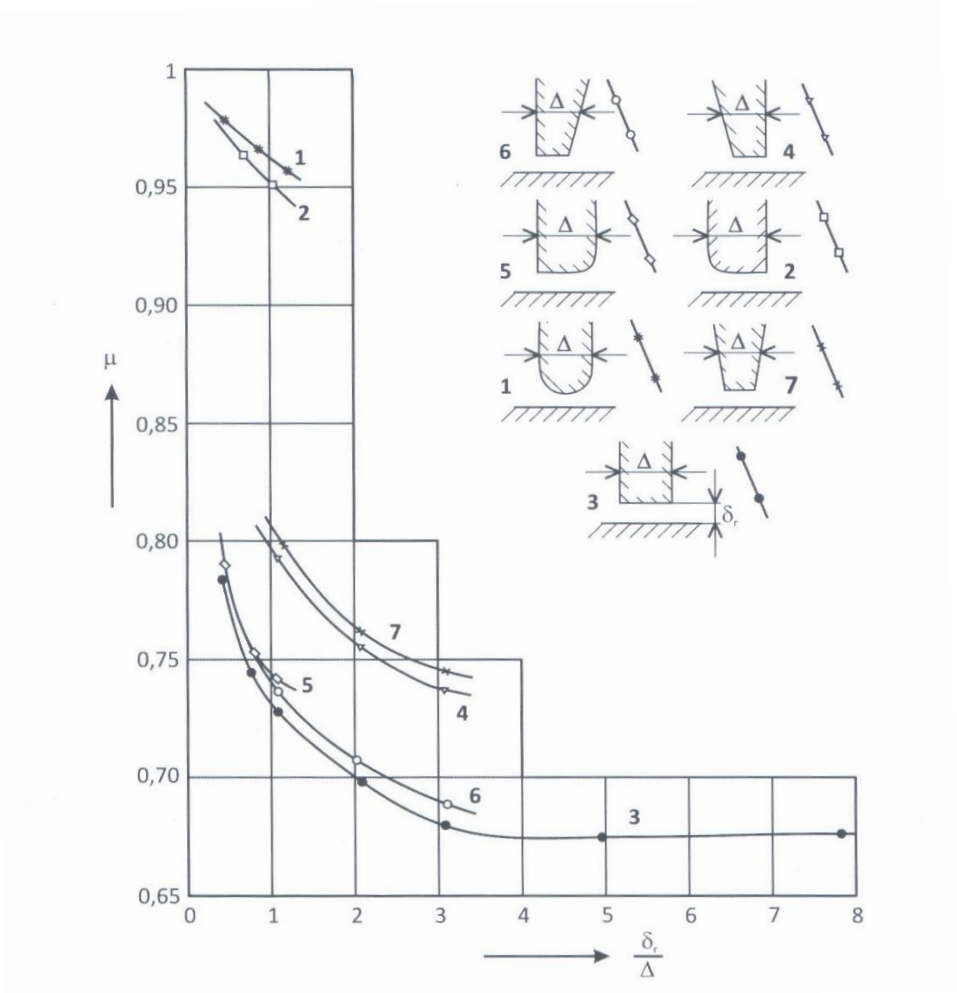

Figure 3-1 The seal contraction ratio [5]

Egli made another major paper on the leakage of steam through labyrinth seals in 1935, where he examined both staggered and see-through configuration of labyrinth seals analytically and experimentally. In his experiments Egli studied the clearances varying from 0,381 mm to 1,016 mm and pressure ratios. These parameters were out of the range in axial turbine applications of the time, but those of interest in modern compressor applications. Egli used Martin's formula, but he took into consideration the fact that the fluid jet undergone a contraction as it goes through tooth clearance. He also took into account the carry over coefficient, which represents the portion of kinetic energy carried over from one cavity to the next. Based on the experimental results and analytical study, he noticed that the percentage of kinetic energy carry over coefficient decreases with increasing spacing between the teeth or with decreasing tooth clearance. Egli through experimental results showed that the carryover effect depends on non-dimensional

clearance to pitch ratio. However he also pointed out that seals with tighter radial clearances ranging from 0,152 mm to 0,254 mm did not have strong dependence on tooth pitch.
[1], [2]

Mass flow seal leakage by Egli:

$$\dot{m} = 2 \cdot \pi \cdot r_{seal} \cdot \delta \cdot C_t \cdot C_C \cdot C_R \cdot \rho_1 \cdot \sqrt{R \cdot T_1} \tag{3-5}$$

or

$$\dot{m} = 2 \cdot \pi \cdot r_{seal} \cdot \delta \cdot C_t \cdot C_C \cdot C_R \cdot \sqrt{\frac{p_1}{v_1}} \tag{3-6}$$

Aungier computed the mass flow leakage through labyrinth seal by the method of Egli in Eq. (3-5) and in Eq. (3-6), in which he provides general empirical equations to approximate coefficients in Egli's equation. The first approximation is the contraction ratio C_r (see Eq. (3-7)) and it depends on clearance to tooth thickness ratio graphically showed in Figure 3-2.

$$C_r = 1 - \frac{1}{3 + \left(\frac{54{,}3}{1 + 100 \cdot \frac{\delta}{t}} \right)^{3{,}45}} \tag{3-7}$$

Egli shows a direct dependence of contraction ratio on tooth thickness as well as on clearance to tooth thickness ratio. *„It seems highly questionable that a dimensional parameter can be used to compute a dimensionless parameter. Indeed, other sources available to this writer suggest that the lower of Egli's two curves should be used for all values of tooth thickness, which is the basis for Eq. (3-7)."*
[6]

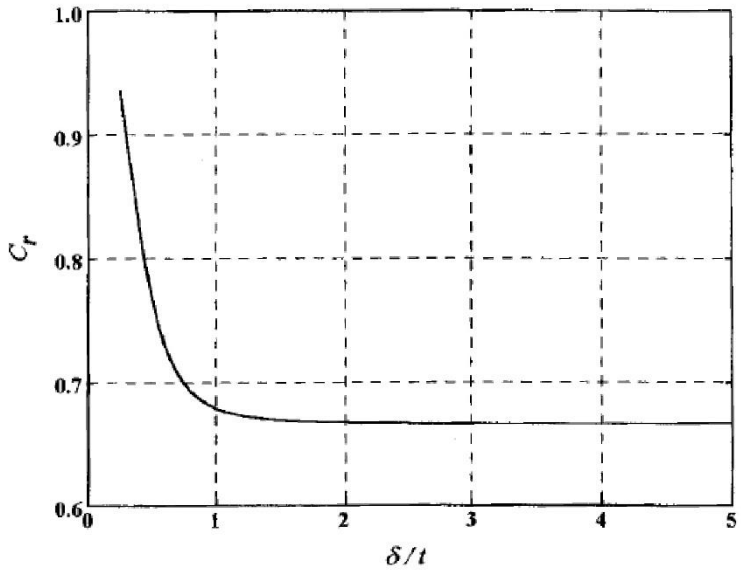

Figure 3-2 The seal throttling coefficient [6]

The throttling coefficient , C_t, is a function of the number of teeth, N, and lower pressure to higher pressure ratio, $P_R=p_2/p_1$, across the labyrinth seal. Figure 3-3 shows the throttling coefficient approximated by :
[6]

$$C_t = \frac{2{,}143[ln(N) - 1{,}464]}{N - 4{,}322} \cdot \left(1 - \frac{p_2}{p_1}\right)^{\left(0{,}375 \cdot \frac{p_2}{p_1}\right)} \qquad (3\text{-}8)$$

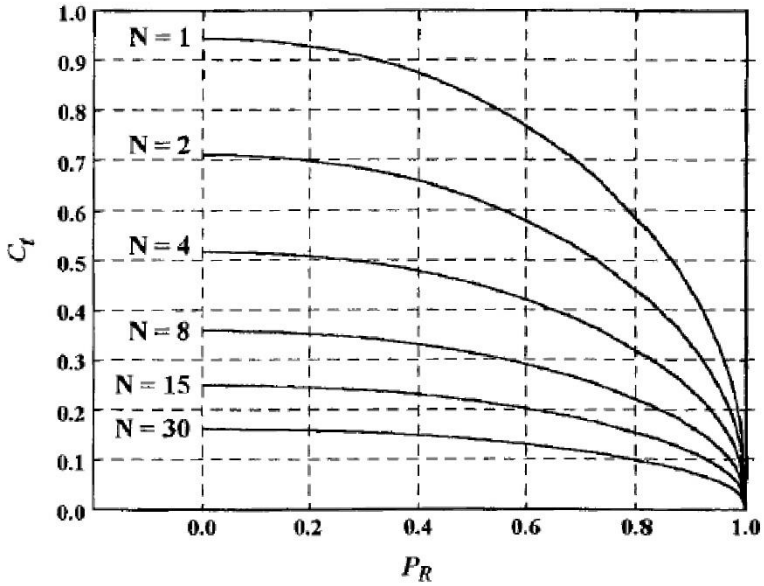

Figure 3-3 The throttling coefficient [6]

The carryover coefficient ,C_c, is a function of the labyrinth seal clearance to the seal pitch ratio. Figure 3-4 shows the carryover coefficient as approximated by:

$$C_c = 1 + \frac{X_1 \cdot \left[\frac{\delta}{p} - X_2 \cdot ln\left(1 + \frac{\delta}{p}\right)\right]}{1 - X_2} \tag{3-9}$$

If N ≤ 12,

$$X_1 = 15{,}1 - 0{,}05255 \cdot e^{[0{,}507 \cdot (12 - N)]} \tag{3-10}$$

$$X_2 = 1{,}058 + 0{,}0218 \cdot N \tag{3-11}$$

If N >12,

$$X_1 = 13{,}15 + 0{,}1625 \cdot N \tag{3-12}$$

$$X_2 = 1{,}32 \tag{3-13}$$

Eq. (3-9) yields a maximum when clearance to pitch ratio is equal to X_2-1, therefore it is wise to require $\delta/p \leq X_2 - 1$ to avoid poor labyrinth seal design. In the case of stepped teeth arrangement the seal radius varies for successive seal teeth and there is no carryover influence, so C_c=1 should be used. [6]

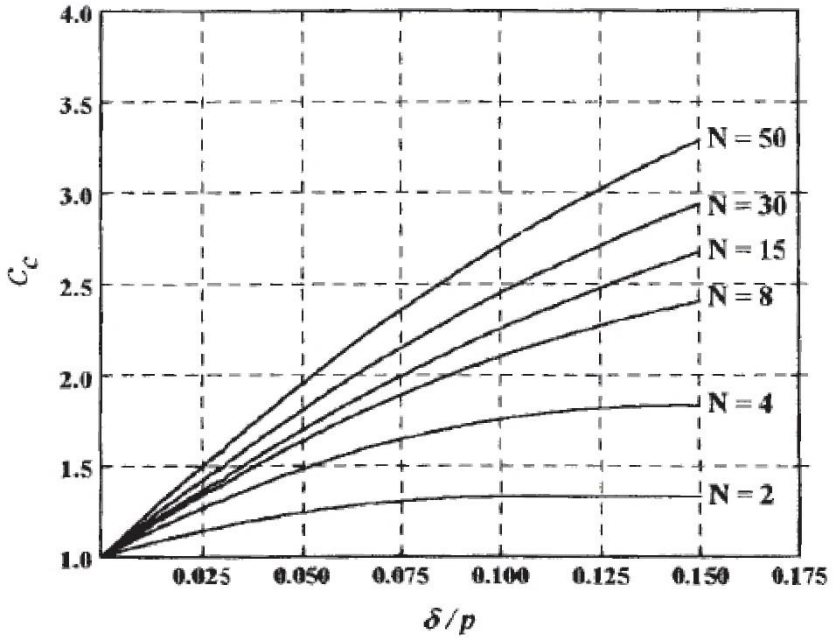

Figure 3-4 The seal carryover coefficient [6]

Professor MEI G.S. Samojlovič derived Eq. (3-14) and Eq. (3-16) to compute the mass flow rate through labyrinth seal.

$$q = \frac{\dot{m}}{\dot{m_{CR}}} = \sqrt{\frac{1 - {\varepsilon_z}^2}{(1 - \varepsilon_{CR}) \cdot n} - \frac{\varepsilon_{CR} \cdot (1 - \varepsilon_z)^2}{(1 - \varepsilon_{CR})^2 \cdot n^2}} \tag{3-14}$$

Similar notation of Eq.(3-14)

$$q = \frac{\dot{m}}{\dot{m_{CR}}} = \sqrt{\frac{1 - \left(\frac{p_2}{p_1}\right)^2}{\left[1 - \left(\frac{p_2}{p_1}\right)_{CR}\right] \cdot n} - \frac{\left(\frac{p_2}{p_1}\right)_{CR} \cdot \left[1 - \left(\frac{p_2}{p_1}\right)\right]^2}{\left[1 - \left(\frac{p_2}{p_1}\right)_{CR}\right]^2 \cdot n^2}} \tag{3-15}$$

Eq. (3-14) enables to evaluate mass flow ratio through labyrinth seal, q, which is increasing with decreasing pressure ratio, ε. To the maximum value of mass flow ratio, q_{max}, is matching the critical mass flow through last constriction referred to critical pressure ratio, $(\varepsilon_{cr})_n$. We set the first derivative of q as a function of ε is equal to zero:

$$(\varepsilon_{CR})_n = \frac{\varepsilon_{CR}}{n \cdot (1 - \varepsilon_{CR}) + \varepsilon_{CR}} \tag{3-16}$$

If the real pressure ratio is lower than the critical pressure ratio, then critical pressure ratio is used to computes mass flow through labyrinth seal. The labyrinth seal shape is not assumed to by sharp, due to abrasive effect during operation and thus the mass flow through constriction increases.

$$\dot{m_{CR}} = \chi \cdot \mu_c \cdot S \cdot \sqrt{\frac{p_1}{v_1}} \tag{3-17}$$

Where χ depends on isoentropic exponent, κ, which is for superheated steam 1,3 and thus χ=0,667 (see Eq. (3-18)).

$$\chi = \sqrt{\kappa \cdot \left(\frac{2}{\kappa+1}\right)^{\frac{\kappa+1}{\kappa-1}}} \tag{3-18}$$

Mass flow calculations mentioned above assumed complete kinetic energy dissipation in each cavity. The carryover coefficient is equal to one. This would be reasonable in case of stepped design, where the steam expands after constriction and also incurvates the steam jet trajectory. The real mass flow through seal includes carryover coefficient (see Figure 3-5) and can be computed by Eq.(3-19) and it is a combination of Eq. (3-15) and Eq. (3-17). The stepped labyrinth teeth is recommended to placed near the axial bearings to avoid the collision between the teeth and the wall, due to shaft movement during heating.
[7], [8]

$$\dot{m} = k_u \cdot \chi \cdot \mu_c \cdot S \cdot \sqrt{\frac{p_1}{v_1}} \cdot \sqrt{\frac{1-\left(\frac{p_2}{p_1}\right)^2}{\left[1-\left(\frac{p_2}{p_1}\right)_{CR}\right] \cdot n} - \frac{\left(\frac{p_2}{p_1}\right)_{CR} \cdot \left[1-\left(\frac{p_2}{p_1}\right)\right]^2}{\left[1-\left(\frac{p_2}{p_1}\right)_{CR}\right]^2 \cdot n^2}} \tag{3-19}$$

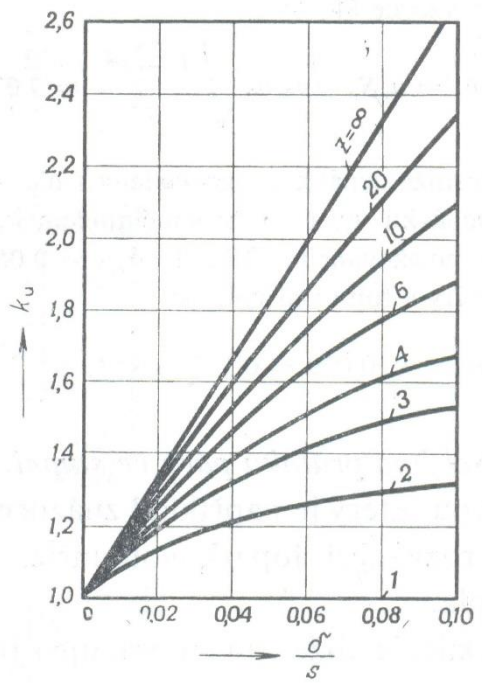

Figure 3-5 Carryover coefficient

Kearton and Keh determined the effects of pressure ratios and different width to clearance ratios on discharge coefficient on a single orifice with zero initial velocity. They implement the correction for the compressibility of the fluid to the Martin's leakage flow model, but they neglected rotation effect of the shaft on the fluid flow leakage, as well as the kinetic energy carryover coefficients. Kearton and Keh compared their analytical formulae with the experimental tests on a 14 throttle staggered labyrinth seals and met the results with fair accuracy.
[1], [4]

$$\dot{m} = k_u \cdot \mu_c \cdot S \cdot \sqrt{\frac{p_1}{v_1}} \cdot \sqrt{\frac{\sum_{i=1}^{n} \varepsilon_i}{n} \cdot \left[\frac{1 - \left(\frac{p_2}{p_1}\right)^2}{n} \right]} \qquad (3\text{-}20)$$

4 RESEARCH OBJECTIVES

Two main objectives of the project had been set up.

The first objective is to build CFD modelling in numerical simulation software which have been specified as ANSYS FLUENT 16.0 and decide what is the sufficient mesh quality of given stepped labyrinth seal geometry (see Figure 4-1), when different boundary conditions and turbulent models are applied, in order to get steady results of mass flow leakage. This objective has been accomplished by applying Finite Volume CFD technique for compressible flow, where three different turbulent models (Standard k-ε model, SST k-ω model and Reynolds stress model) were used for specified boundary conditions of high pressure steam turbine parameters at inlet and outlet of given labyrinth seal.

The second objective is to evaluate mass flow leakage by applying existing leakage models and find the relation with numerical results from ANSYS FLUENT 16.0. Then decide what simulation results correlate with analytical data the most and run the simulations for wide range of pressure ratios.

The result of this paper is to verify the accuracy of the empirical relationships using CFD calculations, as well as it should provide suggestions to the designers in terms of sufficient mesh quality and what turbulent model is better to use for CFD simulations in similar applications (boundary conditions and geometries of labyrinth seals). [9]

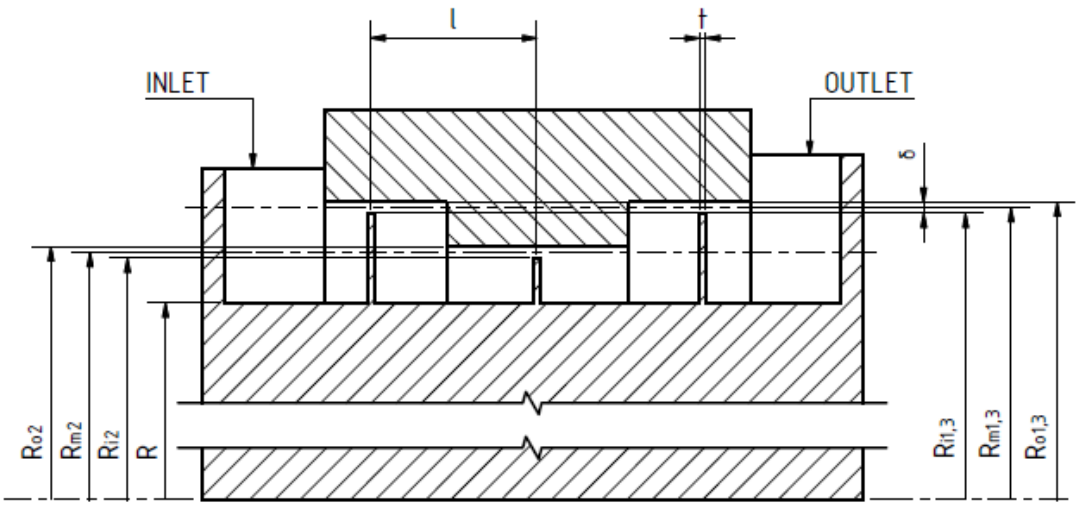

Figure 4-1 Design of labyrinth seal

5 CALCULATION OF EXISTING LEAKAGE MODELS

In the research were used four different existing models (Stodola, Aungier, Samoylovich, Kearton) to evaluate mass flow leakage through given geometry of labyrinth seals with the tooth mounted on the rotor (see Figure 4-1, see Table 5-1). To all of the models can be applied that carryover coefficient, k_u, is equal to 1 due to stepped design of labyrinth seal. Mean value, μ, is 0,71 in order to include shape of the teeth and dimensions of clearance between teeth and stator are taken into account.

Table 5-1 Given dimensions of labyrinth seal

SEAL GEOMETRY				
DIMENSION	TOOTH			UNITS
	1	2	3	
R_o	190	188	190	mm
R_i	189,5	187,5	189,5	mm
R_m	189,75	187,75	189,75	mm
t = Δ		0,3		mm
l		7,4		mm
δ		0,5		mm
h	4	2	4	mm

Average clearance radius between tooth and the stator wall:

$$R_m = \frac{R_{m1} + R_{m2} + R_{m3}}{3} = \frac{189{,}75 + 187{,}75 + 189{,}75}{3}$$
$$R_m = 189{,}083\ mm \tag{5-1}$$

Average clearance Area between tooth and the stator wall:

$$S = 2 \cdot \pi \cdot R_m \cdot \delta = 2 \cdot \pi \cdot 189{,}083 \cdot 0{,}5$$
$$S = 594{,}023\ mm^2 \tag{5-2}$$

Clearance to tooth thickness ratio:

$$\frac{\delta}{\Delta} = \frac{0{,}5}{0{,}3} = 1{,}667\ [-] \tag{5-3}$$

Parameters of high pressure steam:

Inlet pressure: p_1= 17800000,00 Pa

Outlet pressure: p_2= 16715384,62 Pa

Inlet temperature: t_1= 847,1 K

Outlet temperature: t_2= 835,2 K

Specific volume at inlet: v= 0,019788093 $m^3 \cdot kg^{-1}$

Isoentropic coefficient: κ= 1,3 [-]

Number of teeth: n= 3

5.1 Samoylovich equation

Mass flow leakage:

$$\dot{m} = k_u \cdot \chi \cdot \mu_c \cdot S \cdot \sqrt{\frac{p_1}{v_1}} \cdot \sqrt{\frac{1 - \left(\frac{p_2}{p_1}\right)^2}{\left[1 - \left(\frac{p_2}{p_1}\right)_{CR}\right] \cdot n} - \frac{\left(\frac{p_2}{p_1}\right)_{CR} \cdot \left[1 - \left(\frac{p_2}{p_1}\right)\right]^2}{\left[1 - \left(\frac{p_2}{p_1}\right)_{CR}\right]^2 \cdot n^2}} =$$

$$= 1 \cdot 0{,}667 \cdot 0{,}71 \cdot 594{,}023 \cdot 10^{-6} \cdot \sqrt{\frac{17{,}8 \cdot 10^6}{0{,}019788093}}$$

$$\cdot \sqrt{\frac{1 - \left(\frac{16715384{,}62}{17{,}8 \cdot 10^6}\right)^2}{[1 - 0{,}546] \cdot 3} - \frac{0{,}546 \cdot \left[1 - \left(\frac{16715384{,}62}{17{,}8 \cdot 10^6}\right)\right]^2}{[1 - 0{,}546]^2 \cdot 3^2}} \quad (5\text{-}4)$$

$$\dot{m} = 2{,}470\ kg \cdot s^{-1}$$

Where χ is:

$$\chi = \sqrt{\kappa \cdot \left(\frac{2}{\kappa + 1}\right)^{\frac{\kappa+1}{\kappa-1}}} = \sqrt{1{,}3 \cdot \left(\frac{2}{1{,}3 + 1}\right)^{\frac{1{,}3+1}{1{,}3-1}}} = 0{,}667 \quad (5\text{-}5)$$

Critical pressure ratio:

$$\varepsilon_{cr} = \left(\frac{p_2}{p_1}\right)_{cr} = \left(\frac{2}{\kappa + 1}\right)^{\frac{\kappa}{\kappa-1}} = \left(\frac{2}{1{,}3 + 1}\right)^{\frac{1{,}3}{1{,}3-1}} = 0{,}546 \quad (5\text{-}6)$$

Critical mass flow leakage ratio

$$q = \frac{\dot{m}}{\dot{m_{CR}}} = \sqrt{\frac{1 - \left(\frac{p_2}{p_1}\right)^2}{\left[1 - \left(\frac{p_2}{p_1}\right)_{CR}\right] \cdot n} - \frac{\left(\frac{p_2}{p_1}\right)_{CR} \cdot \left[1 - \left(\frac{p_2}{p_1}\right)\right]^2}{\left[1 - \left(\frac{p_2}{p_1}\right)_{CR}\right]^2 \cdot n^2}}$$

$$q = \frac{\dot{m}}{\dot{m_{CR}}} = \sqrt{\frac{1 - \left(\frac{16715384{,}62}{17{,}8 \cdot 10^6}\right)^2}{[1 - 0{,}546] \cdot 3} - \frac{0{,}546 \cdot \left[1 - \left(\frac{16715384{,}62}{17{,}8 \cdot 10^6}\right)\right]^2}{[1 - 0{,}546]^2 \cdot 3^2}} \quad (5\text{-}7)$$

$$q = \frac{\dot{m}}{\dot{m_{CR}}} = 0{,}293\ kg \cdot s^{-1}$$

5.2 Stodola equation

Mass flow leakage:

$$\dot{m} = \mu_c \cdot S \cdot \sqrt{\frac{{p_1}^2 - {p_2}^2}{p_1 \cdot v_1 \cdot n}}$$

$$\dot{m} = 0{,}71 \cdot 594{,}023 \cdot 10^{-6} \cdot \sqrt{\frac{(17{,}8 \cdot 10^6)^2 - (16715384{,}62)^2}{17{,}8 \cdot 10^6 \cdot 0{,}019788093 \cdot 3}} \quad (5\text{-}8)$$

$$\dot{m} = 2{,}510\ kg \cdot s^{-1}$$

Critical mass flow leakage ratio

$$\frac{\dot{m}}{\dot{m}_{cr}} = \mu_c \cdot \sqrt{\frac{1 - \frac{{p_2}^2}{{p_1}^2}}{\kappa \cdot z} \cdot \left(\frac{2}{\kappa + 1}\right)^{\frac{\kappa+1}{1-\kappa}}}$$

$$\frac{\dot{m}}{\dot{m}_{cr}} = 0{,}71 \cdot \sqrt{\frac{1 - \frac{16715384{,}62^2}{(17{,}8 \cdot 10^6)^2}}{1{,}3 \cdot 3} \cdot \left(\frac{2}{1{,}3 + 1}\right)^{\frac{1{,}3+1}{1-1{,}3}}} \quad (5\text{-}9)$$

$$\frac{\dot{m}}{\dot{m}_{cr}} = 0{,}211\ kg \cdot s^{-1}$$

5.3 Aungier equation

Mass flow leakage:

$$\dot{m} = 2 \cdot \pi \cdot r_{seal} \cdot \delta \cdot C_t \cdot C_C \cdot C_R \cdot \sqrt{\frac{p_1}{v_1}}$$

$$\dot{m} = 594{,}023 \cdot 10^{-6} \cdot 0{,}221 \cdot 0{,}669 \cdot \sqrt{\frac{17{,}8 \cdot 10^6}{0{,}019788093}} = 2{,}635\ kg \cdot s^{-1} \quad (5\text{-}10)$$

Where The throttling coefficient , C_t, is:

$$C_t = \frac{2{,}143[ln(3) - 1{,}464]}{3 - 4{,}322} \cdot \left(1 - \frac{16715384{,}62}{17{,}8 \cdot 10^6}\right)^{\left(0{,}375 \cdot \frac{16715384{,}62}{17{,}8 \cdot 10^6}\right)} \quad (5\text{-}9)$$

$$C_t = 0{,}221\ [-]$$

The contraction ratio C_r is:

$$C_r = 1 - \frac{1}{3 + \left(\frac{54{,}3}{1 + 100 \cdot \frac{\delta}{t}}\right)^{3{,}45}} = 1 - \frac{1}{3 + \left(\frac{54{,}3}{1 + 100 \cdot \frac{0{,}5}{0{,}3}}\right)^{3{,}45}} \quad (5\text{-}10)$$

$$C_r = 0{,}669\ [-]$$

Critical mass flow leakage ratio

$$\frac{\dot{m}}{\dot{m}_{cr}} = \frac{2 \cdot \pi \cdot r_{seal} \cdot \delta \cdot C_t \cdot C_C \cdot C_R \cdot \sqrt{\frac{p_1}{v_1}}}{\sqrt{\kappa \cdot \left(\frac{2}{\kappa + 1}\right)^{\frac{\kappa+1}{\kappa-1}} \cdot S \cdot \sqrt{\frac{p_1}{v_1}}}}$$

$$\frac{\dot{m}}{\dot{m}_{cr}} = \frac{C_t \cdot C_C \cdot C_R}{\sqrt{\kappa \cdot \left(\frac{2}{\kappa + 1}\right)^{\frac{\kappa+1}{\kappa-1}}}} \quad (5\text{-}11)$$

$$\frac{\dot{m}}{\dot{m}_{cr}} = \frac{1 \cdot 0{,}221 \cdot 0{,}669}{\sqrt{1{,}3 \cdot \left(\frac{2}{1{,}3 + 1}\right)^{\frac{1{,}3+1}{1{,}3-1}}}} = 0{,}222\ kg \cdot s^{-1}$$

5.4 Kearton equation

Mass flow leakage:

$$\dot{m} = k_u \cdot \mu_c \cdot S \cdot \sqrt{\frac{p_1}{v_1}} \cdot \sqrt{\frac{\sum_{i=1}^{n} \varepsilon_i}{n} \cdot \left[\frac{1 - \left(\frac{p_2}{p_1}\right)^2}{n}\right]} \tag{5-12}$$

$$\dot{m} = 1 \cdot 0{,}71 \cdot 594{,}023 \cdot 10^{-6} \cdot \sqrt{\frac{17{,}8 \cdot 10^6}{0{,}019788093}} \cdot \sqrt{\frac{2{,}938}{3} \cdot \left[\frac{1 - \left(\frac{16715384{,}62}{17{,}8 \cdot 10^6}\right)^2}{3}\right]}$$

$$\dot{m} = 2{,}484\ kg \cdot s^{-1}$$

Pressure after each tooth:

$$p_{ti} = \sqrt{{p_1}^2 - \frac{i}{n} \cdot ({p_1}^2 - {p_2}^2)}$$

$$p_{t1} = \sqrt{17{,}8 \cdot 10^{6^2} - \frac{1}{3} \cdot \left(17{,}8 \cdot 10^{6^2} - 16715384{,}62^2\right)} \tag{5-13}$$

$$p_{t1} = 17445955{,}43\ Pa$$

$$p_{t2} = \sqrt{17{,}8 \cdot 10^{6^2} - \frac{2}{3} \cdot \left(17{,}8 \cdot 10^{6^2} - 16715384{,}62^2\right)} = 17084575{,}56\ Pa$$

Pressure ratio on each tooth:

$$\varepsilon_i = \frac{p_i}{p_{i-1}}$$

$$\varepsilon_1 = \frac{p_{t1}}{p_1} = \frac{17445955{,}43}{17800000} = 0{,}980\ [-]$$

$$\varepsilon_2 = \frac{p_{t2}}{p_{t1}} = \frac{17084575{,}56}{17445955{,}43} = 0{,}979\ [-] \tag{5-14}$$

$$\varepsilon_3 = \frac{p_2}{p_{t2}} = \frac{16715384{,}62}{17084575{,}56} = 0{,}978\ [-]$$

$$\sum_{i=1}^{n} \varepsilon_i = \varepsilon_1 + \varepsilon_2 + \varepsilon_3 = 0{,}980 + 0{,}979 + 0{,}978 = 2{,}938$$

Critical mass flow leakage ratio

$$\frac{\dot{m}}{\dot{m}_{cr}} = \frac{k_u \cdot \mu_c \cdot S \cdot \sqrt{\frac{p_1}{v_1}} \cdot \sqrt{\frac{\sum_{i=1}^{n} \varepsilon_i}{n} \cdot \left[\frac{1 - \left(\frac{p_2}{p_1}\right)^2}{n}\right]}}{\sqrt{\kappa \cdot \left(\frac{2}{\kappa+1}\right)^{\frac{\kappa+1}{\kappa-1}}} \cdot S \cdot \sqrt{\frac{p_1}{v_1}}}$$

$$\frac{\dot{m}}{\dot{m}_{cr}} = \frac{k_u \cdot \mu_c \cdot S \cdot \sqrt{\frac{p_1}{v_1}} \cdot \sqrt{\frac{\sum_{i=1}^{n} \varepsilon_i}{n} \cdot \left[\frac{1 - \left(\frac{p_2}{p_1}\right)^2}{n}\right]}}{\sqrt{\kappa \cdot \left(\frac{2}{\kappa+1}\right)^{\frac{\kappa+1}{\kappa-1}}} \cdot S \cdot \sqrt{\frac{p_1}{v_1}}}$$

$$\frac{\dot{m}}{\dot{m}_{cr}} = \frac{k_u \cdot \mu_c \cdot \sqrt{\frac{\sum_{i=1}^{n} \varepsilon_i}{n} \cdot \left[\frac{1 - \left(\frac{p_2}{p_1}\right)^2}{n}\right]}}{\sqrt{\kappa \cdot \left(\frac{2}{\kappa+1}\right)^{\frac{\kappa+1}{\kappa-1}}}} \qquad (5\text{-}15)$$

$$\frac{\dot{m}}{\dot{m}_{cr}} = \frac{1 \cdot 0{,}71 \cdot \sqrt{\frac{2{,}938}{3} \cdot \left[\frac{1 - \left(\frac{16715384{,}62}{17{,}8 \cdot 10^6}\right)^2}{3}\right]}}{\sqrt{1{,}3 \cdot \left(\frac{2}{1{,}3+1}\right)^{\frac{1{,}3+1}{1{,}3-1}}}}$$

$$\frac{\dot{m}}{\dot{m}_{cr}} = 0{,}209\ kg \cdot s^{-1}$$

5.5 Zalf equation

Mass flow leakage:

$$\dot{m} = 1{,}5 \cdot \chi \cdot S \cdot \sqrt{\frac{p_1}{v_1}} \cdot \sqrt{\frac{1 - \left(\frac{p_2}{p_1}\right)^2}{n - \ln\left(\frac{p_2}{p_1}\right)}} \tag{5-16}$$

$$\dot{m} = 1{,}5 \cdot 0{,}667 \cdot 594{,}023 \cdot 10^{-6} \cdot \sqrt{\frac{17{,}8 \cdot 10^6}{0{,}019788093}} \cdot \sqrt{\frac{1 - \left(\frac{16715384{,}62}{17{,}8 \cdot 10^6}\right)^2}{3 - \ln\left(\frac{16715384{,}62}{17{,}8 \cdot 10^6}\right)}}$$

$$\dot{m} = 3{,}502\ kg \cdot s^{-1}$$

Table 5-2 Summary of existing leakage model results

SUMMARY OF EXISTING LEAKAGE MODELS CALCULATION	
CALCULATION	Mass flow leakage [kg/s]
SAMOYLOVICH	2,469573
STODOLA	2,510343
AUNGIER	2,635235
KEARTON	2,484177
ZALF	3,502346

6 NUMERICAL CALCULATION

6.1 Introduction

The current research is mostly based upon CFD simulations of steam flow through labyrinth seals, performed using the commercial CFD code FLUENT 16.0. The variation of the seal shape on the flow pattern through labyrinth seal is not accommodated to this research based on fixed dimensions. An extensive study, which is not only time consuming, but also expensive if done experimentally, can be performed using numerical method of fluid flow behaviour. There are few assumptions made to reduce the computational time in current research. These assumptions are:

A. The flow and geometry are assumed to be axisymmetric and hence a two dimensional instead of three dimensional simulation is utilized.

B. Fluid surface interaction (FSI) has not been taken in to account the surface roughness of the seal geometry.

C. The shapes variations of the geometry due to thermal stress defining the fluid flow path are negligible.

In this work commercial solver FLUENT 16.0 has been employed to solve the fundamental governing equations of thermo-fluid sciences. It uses the finite volume method for discretization. Simulations are performed with ideal gas. The standard k-ε, Reynolds stress and SST k-ω turbulent models were used to simulate the ideal gas flow. Mathematical details on turbulent models mentioned above are described in following subsection. [1],[4]

6.2 Governing equations

The Navier - Stokes equations are equations can be used to determine the velocity vector field that applies to a fluid, given some initial conditions. The Navier-Stokes equations, developed by Claude-Louis Navier and George Gabriel Stokes in 1822, arise from the basic principle of conservation of momentum (Eq.6-8), mass (Eq.6-7) and energy (Eq.6-9). In order to derive the equations of fluid motion, we must first derive the continuity equation (see Eq.6-6). It dictates condition under which things are conserved. Then apply the equation to conservation of mass and momentum and combine them with a physical understanding of what a fluid is.

For almost all real situations, they result in a system of nonlinear partial differential equations of second order, however in case of one dimensional motion can be reduced to linear differential equations. Usually, however, they remain nonlinear and even for their formal simplicity, it makes them difficult to solve. Untill today it has not been proven the existence of their analytical solution. For the compressible Newtonian fluid Navier – Stokes equation yields to:

$$\rho \cdot \left(\frac{\partial \boldsymbol{v}}{\partial t} + \boldsymbol{v} \cdot \nabla \boldsymbol{v}\right) = -\nabla p + \nabla \cdot \left\{\mu[\nabla \mathbf{v} + (\nabla \mathbf{v})^T] - \frac{2}{3}\mu \cdot (\nabla \boldsymbol{v}) \cdot \boldsymbol{I}\right\} + F \qquad (6\text{-}1)$$

Single parts of equation has a following meaning:

Inertial forces: $$\rho \cdot \left(\frac{\partial \boldsymbol{v}}{\partial t} + \boldsymbol{v} \cdot \nabla \boldsymbol{v}\right) \qquad (6\text{-}2)$$

Pressure forces: $$-\nabla p \qquad (6\text{-}3)$$

Viscous forces: $$\nabla \cdot \left\{\mu[\nabla \mathbf{v} + (\nabla \mathbf{v})^T] - \frac{2}{3}\mu \cdot (\nabla \boldsymbol{v}) \cdot \boldsymbol{I}\right\} \qquad (6\text{-}4)$$

External forces applied to the fluid: $F = \boldsymbol{\rho} \cdot g$ (6-5)

$$\frac{\partial \boldsymbol{\rho}}{\partial t} + \nabla \cdot (\boldsymbol{\rho} \cdot \boldsymbol{v}) = 0 \qquad (6\text{-}6)$$

Where ρ is the fluid density, v is the fluid velocity, p is the fluid pressure and μ is the dynamic viscosity of the fluid. [13],[14],[15]

Mass conservation equation- 2D:

$$\frac{\partial \rho}{\partial t} + \frac{\partial}{\partial x}(\rho v_x) + \frac{\partial}{\partial r}(r v_r) + \frac{\rho v_r}{r} = S_m \quad (6\text{-}7)$$

Momentum conservation equation for swirl velocity:

$$\frac{\partial}{\partial t}(\rho w) + \frac{1}{r}\frac{\partial}{\partial x}(r\rho u w) + \frac{1}{r}\frac{\partial}{\partial r}(r\rho v w) = \frac{1}{r}\frac{\partial}{\partial x}\left[r\mu\frac{\partial w}{\partial x}\right] + \frac{1}{r^2}\frac{\partial}{\partial r}\left[r^3\mu\frac{\partial}{\partial r}\left(\frac{w}{r}\right)\right] - \rho\frac{vw}{r} \quad (6\text{-}8)$$

Energy conservation

$$\frac{\partial}{\partial t}\cdot(\boldsymbol{\rho}\cdot\boldsymbol{E}) + \nabla\cdot\left(\vec{\boldsymbol{v}}\cdot(\rho\cdot E + p)\right) = -\nabla\cdot\left(\sum_j h_j\cdot J_j\right) + \boldsymbol{S_h} \quad (6\text{-}9)$$

Where S_m is mass added to the continuous phase from the dispersed second phase,x is the axial coordinate,r is the radial coordinate,u is the axial velocity,v is the radial velocity and w is the swirl velocity. [15]

6.2.1 Turbulent models

Mathemtical modeling of turbulent flows aim to realisticly simulate flows and predict their motion, which will often be turbulent. Due to the random structure of turbulence we cannot perfectly represent the effects of turbulence in CFD even after a century of research in this field, there are no successful universal turbulence model available. Therefore the choice of turbulence model plays an important role on the accuracy of CFD predictions. Turbulent models used in this paper are described below. [17]

6.2.1.1 Standard k-ε model

Standard k-ε model has become widely used model for engineering applications, due to his simplicity and sufficient accuracy. This model is based on the equations for the turbulence kinetic energy, k, and its dissipation rate, ε. The k-ε model is the most appropriate viscous model for numerical simulation of high Reynolds number (fully developed turbulent flow), however accuracy of the results decrease with increasing pressure gradients.

Equation of k-ε model:

$$\frac{\partial}{\partial t}(\rho k) + \frac{\partial}{\partial x_i}(\rho k u_i) = \frac{\partial}{\partial x_j}\left[\left(\mu + \frac{\mu_t}{\sigma_k}\right)\frac{\partial k}{\partial x_j}\right] + G_k + G_b - \rho\varepsilon - Y_M + S_k \quad (6\text{-}10)$$

And

$$\frac{\partial}{\partial t}(\rho \varepsilon) + \frac{\partial}{\partial x_i}(\rho k u_i) = \frac{\partial}{\partial x_j}\left[\left(\mu + \frac{\mu_t}{\sigma_\varepsilon}\right)\frac{\partial \varepsilon}{\partial x_j}\right] + C_{1\varepsilon}\frac{\varepsilon}{k}(G_k + C_{3\varepsilon}G_b) - C_{2\varepsilon}\rho\frac{\varepsilon^2}{k} + S_\varepsilon \quad (6\text{-}11)$$

In these equations term, G_k, represents the generation of turbulence kinetic energy due to the mean velocity gradients and it is defined as:

$$G_k = -\rho \cdot \overline{u_\iota \cdot u_j}\frac{\partial u_j}{\partial x_i} \quad (6\text{-}12)$$

The term, G_b, is the production of turbulence kinetic energy due to buoyancy, calculated as described:

$$G_b = \beta \cdot g_i \cdot \frac{\mu_t \cdot \partial T}{Pr_t \cdot \partial x_i} \quad (6\text{-}13)$$

Y_M is the contribution of the fluctuating dilatation in compressible turbulence to the overall dissipation rate, ε, calculated as shown below:

$$Y_M = 2 \cdot \rho \cdot \varepsilon \cdot M_t^2 = 2 \cdot \rho \cdot \varepsilon \cdot \frac{k}{a^2} \cong 2 \cdot \rho \cdot \varepsilon \cdot \frac{k}{\gamma \cdot R_g \cdot T} \quad (6\text{-}14)$$

$C_{1\varepsilon}$, $C_{2\varepsilon}$ and $C_{3\varepsilon}$, are constants with default values $C_{1\varepsilon}$ =1,44 and $C_{2\varepsilon}$ =1,92. σ_k, and σ_ε, are the turbulent Prandtl numbers for the turbulence kinetic energy(σ_k=1) and its dissipation rate(σ_ε=1,3). S_k and S_ε are defined source terms by user. The values mentioned above were used as default setting in this research for Standard k-ε model. [1] ,[15]

6.2.1.2 Shear-Stress Transport (SST) k-ω Model

The SST k-ω model was developed in 1993 by Menter to effectively combine the robust and accurate formulation of the k-ω model in the near wall region with the free stream independence of the k-ε model in the far field and thereby avoids the common k-ω model problem, which is high sensitivity to the inlet free stream turbulence properties. To achieve this, the k-ε model is converted into k-ω model formulation, where the transported variable, k, is kinetic energy and it determines the energy in the turbulence. To determine the scale of the turbulence the variable of the specific dissipation, ω, is used. The SST k-ω model includes following refinements in comparison with Standard k-ω model:

A. *„The standard k-ω model and the transformed k-ε model are both multiplied by a blending function and both models are added together. The blending function is designed to be one in the near-wall region, which activates the standard k-ω model, and zero away from the surface witch activates the transformed k-ε model." [15]*

B. The damped cross diffusion derivative term in the ω equation is incorporated to the SST model.

C. Different modelling constants.

D. The turbulent viscosity definition is modified to account for the transport of the turbulent shear stress.

These features makes the SST model more accurate and reliable for a wider class of flows than the Standard model. The SST k-ω model is beneficial to use for adverse high pressure gradients and separating flow.

Equation of SST k-ω model:

$$\frac{\partial}{\partial t}(\rho k) + \frac{\partial}{\partial x_i}(\rho k u_i) = \frac{\partial}{\partial x_j}\left[\Gamma_k \frac{\partial k}{\partial x_j}\right] + G_k - Y_k + S_k \qquad (6\text{-}15)$$

And

$$\frac{\partial}{\partial t}(\rho\omega) + \frac{\partial}{\partial x_i}(\rho\omega u_i) = \frac{\partial}{\partial x_j}\left[\Gamma_\omega \frac{\partial \omega}{\partial x_j}\right] + G_\omega - Y_\omega + D_\omega + S_\omega \quad (6\text{-}16)$$

The term, G_k, represents the production of turbulence kinetic energy. G_ω, represents the generation of specific dissipation, ω, as it is shown below:

$$G_\omega = \alpha \cdot \frac{\omega}{k} \cdot G_k \quad (6\text{-}17)$$

The effective diffusity of k and ω are represented by Γk and Γω, as calculated below:

$$\Gamma_k = \mu + \frac{\mu_t}{\sigma_k} \quad (6\text{-}18)$$

$$\Gamma_\omega = \mu + \frac{\mu_t}{\sigma_\omega} \quad (6\text{-}19)$$

The terms Y_k and Y_ω describes the dissipation of k and ω due to turbulence and it is calculated as described in to the overall dissipation rate, ε, calculated as shown below:

$$Y_k = \rho \cdot \beta^* \cdot f_{\beta*} \cdot k \cdot \omega \quad (6\text{-}20)$$

$$Y_\omega = \rho \cdot \beta \cdot f_\beta \cdot \omega^2 \quad (6\text{-}21)$$

The cross diffusion term D_ω:

$$D_\omega = 2 \cdot (1 - F_1) \cdot \rho \cdot \frac{1}{\omega \cdot \sigma_{\omega,2}} \cdot \frac{\partial k}{\partial x_j} \cdot \frac{\partial \omega}{\partial x_j} \quad (6\text{-}22)$$

S_k and S_ε are defined source terms by user. [15]

6.2.1.3 Reynolds Stress Model (RSM)

The RSM is the most elaborated RANS turbulent model that abandons the isotropic eddy-viscosity hypothesis and closes the Reynolds averaged Navier-Stokes equations by solving transport equations for the Reynolds stresses, together with an equation for the dissipation rate. This means that seven additional transport equations are required in 3D. Since the RSM accounts for the effects of streamline curvature, rotation, swirl and rapid changes in strain rate in a more rigorous mannes than models using one or two equations. Even it has greater potenial to accuratly predict complex flows, the fidelity of the RSM is still limited by tle closure assumptions employed to model various terms in the exact transport equations. The modeling of the dissipation rate and pressure strain terms is challenging task and it is often considered to be responsible for compromising the accuracy of Reynold Stress Model predictions. RSM also relies on scale equations ε and ω.

The Reynolds Stress Model equation:

$$\frac{\partial}{\partial t}\left(\rho\overline{u_i'u_j'}\right)+\frac{\partial}{\partial x_k}\left(\rho u_k\overline{u_i'u_j'}\right)=-\frac{\partial}{\partial x_k}\left[\rho\overline{u_i'u_j'u_k'}+\overline{p\left(\delta_{kj}u_i'+\delta_{ik}u_j'\right)}\right]+$$
$$\frac{\partial}{\partial x_k}\left[\mu\frac{\partial}{\partial x_k}\left(\overline{u_i'u_j'}\right)\right]-\rho\left(\overline{u_i'u_k'}\frac{\partial u_j}{\partial x_k}+\overline{u_j'u_k'}\frac{\partial u_i}{\partial x_k}\right)-\beta\rho\left(g_i\overline{u_j'\theta}+g_j\overline{u_i'\theta}\right)+ \quad (6\text{-}23)$$
$$p'\left(\frac{\partial u_i'}{\partial x_j}+\frac{\partial u_j'}{\partial x_i}\right)-2\mu\overline{\frac{\partial u_i'}{\partial x_k}\frac{\partial u_j'}{\partial x_k}}-2\rho\Omega_k\left(\overline{u_j'u_m'}\varepsilon_{ikm}+\overline{u_i'u_m'}\varepsilon_{jkm}\right)+S_{user}$$

Single parts of equation has a following meaning:

Local time derivative: $$\frac{\partial}{\partial t}\left(\rho\overline{u_i'u_j'}\right) \quad (6\text{-}24)$$

Convection: $$\frac{\partial}{\partial x_k}\left(\rho u_k\overline{u_i'u_j'}\right) \quad (6\text{-}25)$$

Turbulent diffusion : $$-\frac{\partial}{\partial x_k}\left[\rho\overline{u_i'u_j'u_k'}+\overline{p\left(\delta_{kj}u_i'+\delta_{ik}u_j'\right)}\right] \quad (6\text{-}26)$$

Molecular diffusion: $$\frac{\partial}{\partial x_k}\left[\mu\frac{\partial}{\partial x_k}\left(\overline{u_i'u_j'}\right)\right] \quad (6\text{-}27)$$

Stress production : $$-\rho\left(\overline{u_i'u_k'}\frac{\partial u_j}{\partial x_k}+\overline{u_j'u_k'}\frac{\partial u_i}{\partial x_k}\right) \quad (6\text{-}28)$$

Buoyancy production: $$-\beta\rho\left(g_i\overline{u_j'\theta}+g_j\overline{u_i'\theta}\right) \quad (6\text{-}29)$$

Pressure strain : $$p' \left(\frac{\partial u_i'}{\partial x_j} + \frac{\partial u_j'}{\partial x_i} \right) \quad (6\text{-}30)$$

Dissipation: $$-2\mu \overline{\frac{\partial u_i'}{\partial x_k} \frac{\partial u_j'}{\partial x_k}} \quad (6\text{-}31)$$

Production by system rotation: $$-2\rho\Omega_k \left(\overline{u_j' u_m'} \varepsilon_{ikm} + \overline{u_i' u_m'} \varepsilon_{jkm} \right) \quad (6\text{-}32)$$

User defined source term: $$S_{user} \quad (6\text{-}33)$$

In these equations the terms C_{ij}, $D_{L,ij}$, P_{ij} and F_{ij} do not require any modelling. However $D_{T,ij}$, G_{ij}, Φ_{ij}, and ε_{ij} need to be modelled to close equation, calculated as described below:

$$D_{T,ij} = \frac{\partial}{\partial x_k} \cdot \left(\frac{\mu_t}{\sigma_k} \frac{\partial \overline{u_i' u_j'}}{\partial x_l} \right) \quad (6\text{-}34)$$

$$\begin{aligned} \emptyset_{ij} = \emptyset_{ij,1} + \emptyset_{ij,2} + \emptyset_{ij,w} = {} & -C_1 \rho \frac{\varepsilon}{k} \left(\overline{u_i' u_j'} - \frac{2}{3}\delta_{ij} k \right) - C_2 \left[\left(P_{ij} + F_{ij} + \right. \right. \\ & \frac{5}{6} G_{ij} - C_{ij} \Big) - \frac{2}{3}\delta_{ij} \left(\frac{1}{2} P_{kk} + \frac{5}{12} G_{kk} - \frac{1}{2} C_{kk} \right) \Big] + C_1' \frac{\varepsilon}{k} \Big(\overline{u_k' u_m'} n_k n_m \delta_{ij} - \\ & \frac{3}{2} \overline{u_i' u_k'} n_j n_k - \frac{3}{2} \overline{u_j' u_k'} n_i n_k \Big) \frac{C_l k^{\frac{3}{2}}}{\varepsilon d} + C_2' \left(\emptyset_{km,2} n_k n_m \delta_{ij} - \frac{3}{2} \emptyset_{ik,2} n_j n_k - \right. \\ & \left. \frac{3}{2} \emptyset_{jk,2} n_i n_k \right) \frac{C_l k^{\frac{3}{2}}}{\varepsilon d} \end{aligned} \quad (6\text{-}35)$$

Where C_1= 1,8, C_1'=0,5 and C_2'=0,3. n_k is the component of the unit normal to the wall, d is the normal distance to the wall.

$$G_{ij} = -\frac{\mu_t}{\rho Pr_t} \cdot \left(g_i \frac{\partial \rho}{\partial x_j} + g_j \frac{\partial \rho}{\partial x_i} \right) \quad (6\text{-}36)$$

$$\varepsilon_{ij} = \frac{2}{3}\delta_{ij} \cdot (\rho\varepsilon + Y_M) \quad (6\text{-}37)$$

[15]

6.3 Meshing

The ANSYS Meshing utility (ANSYS Workbench 16.0) has been used to create the grid of labyrinth seal. The two dimensional simulation is utilized by assuming the geometry and fluid flow to be axisymmetric. The detailed dimensions are shown in Figure 6-1. Due to the division of seal in to specific areas and using geometric series distribution of quadrilateral cells (see Eq.6-38), the mesh become more dense in the clearance and wall regions (Figure 6-2). The resolution of grid was controled by changing initial cell length, a_0, from 10^{-1} to 10^{-4} mm and growth rate, q, equals to 1,2. Additionaly was run simulation with scale factor 1,1 and a_0, eqeualed to 10^{-4} mm, in order to resolve eddies in the low middle dense cell areas and monitor the effect on mass flow leakage.

$$n = \frac{2 \cdot ln\left[\frac{D}{2} \cdot \frac{(q-1)}{a_0} + 1\right]}{ln(q)} \tag{6-38}$$

Where, n, is number of divisions of specified area. The term D is distance of each area. The growth rate q and initial cell length a_0. The grid specification calculated from Eq. 6-35 are described in *Appendix A*.

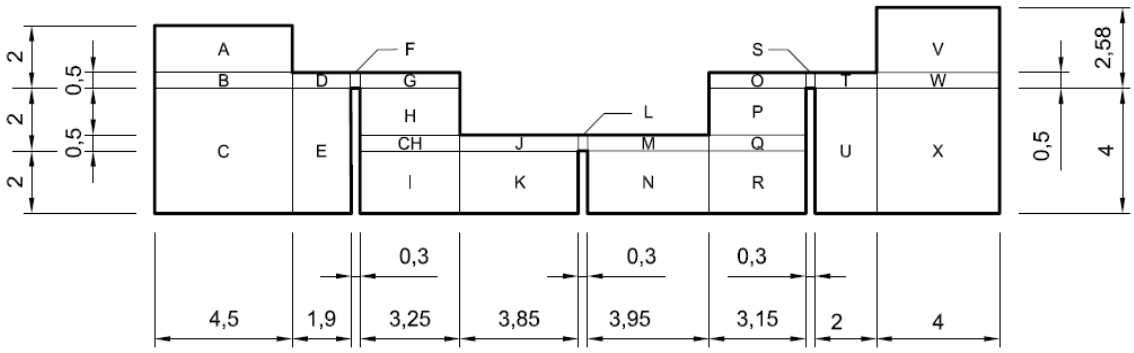

Figure 6-1 Labyrinth seal dimensions

Figure 6-2 Mesh density

The Ansys Workbench 16.0 provides other mathematical tools to check and classify quality of created mesh. One of them is skewness value, which describes the difference between shape of the cell and shape of an equilateral cell of equivalent volume. According to Ansys fluent user guide different cell quality can be indexed by different range of skewness value (see Table 6-1).

Table 6-1 Skewness range

Skewness	Cell quality
1	degenerate
0,9 - <1	bad
0,75 - 0,9	poor
0,5 - 0,75	fair
0,25 - 0,5	good
>0 - 0,25	excellent
0	equilateral

The ratio between length of the longest edge and the length of the shortest edge is called Aspect ratio and it is another value how to index mesh quality. The mesh quality is considered to be good if value of single precision Aspect ratio is less than one hundred or less than ten thousand for double precision Aspect ratio . The last mentioned control index of mesh quality is called Minimum orthogonal quality and it is in the range from 0 to 1, where 0 is the worst and 1 is the best value. It can be computed using the face normal vector , the vector from the cell centroid to each faces and vector from the cell centroid of each to the adjacent cells. As you can see in Table 6-2, the mesh quality based on these three parameters is very good.

The results of any discretized solution is dependent on the quality and length scale of the constituent elements. CFD analysis are particularly prone to numerical discretization error, therefore it is important that the grid independence be considered before critical review of CFD results. Grid independence was the main objective of this project and it was performed by running several solutions with grids of increasing quality, when different turbulent models were applied. The results of mass flow rates predicted for various pressure ratios are compared and grid independence is achieved when the solution does not change appreciably as a grid

quality is changed. However the highest resolution of the grid was set to $a_0=10^{-4}$ mm, in order to decrease the solving time. [4],[9],[16]

Table 6-2 Mesh quality parameters

Mesh no.	q	a_0	Nodes	Maximum Orthogonal Skewness	Minimum Orthogonal Quality	Maximum Aspect Ratio
	[-]	[mm]	[-]	[-]	[-]	[-]
1	1,2	10^{-1}	3 556	$1{,}20575\cdot10^{-8}$	1	4,78862
2	1,2	$5\cdot10^{-2}$	7 382	$4{,}50648\cdot10^{-8}$	1	8,12178
3	1,2	10^{-2}	25 552	$1{,}00349\cdot10^{-6}$	0,999999	26,3631
4	1,2	$5\cdot10^{-3}$	37 965	$3{,}27050\cdot10^{-6}$	0,999997	41,7642
5	1,2	10^{-3}	79 149	$2{,}87492\cdot10^{-5}$	0,999971	78,4186
6	1,2	$5\cdot10^{-4}$	99 521	$1{,}12885\cdot10^{-5}$	0,999989	83,8170
7	1,2	10^{-4}	165 526	$9{,}25412\cdot10^{-5}$	0,999907	75,9438
8	1,1	10^{-4}	496 571	$2{,}05018\cdot10^{-5}$	0,999979	39,2395

6.4 Fluent solver settings

CFD solutions were generated using ANSYS Fluent 16.0. Table 6-3 provides details regarding the Fluent solver settings and modelling options employed.

Table 6-3 Summary of Fluent solver setting

FLUENT CFD settings	Value
Solver type	Pressure based
Velocity formulation	Absolute
Turbulence Model	Standard k-ε model k-ω SST Reynolds stress
Wall function	Scalable
Material	Ideal gas
Solution scheme	Simple
Spatial discretization - Gradient	Least squares cell based
Spatial discretization - Pressure	Second order
Spatial discretization – Density, Momentum, Sqirl velocity, Energy	Second order upwind
Spatial discretization – Turbulent kinetic energy, turbulent dissipation rate	Second order upwind
Number of iteration	Up to 100 000

6.5 Mesh and turbulent model selection

A 2D axisymmetric model was used to investigate the leakage rates in steam turbine. As iterations are performed, monitor physical quantities of interest are tracked for steady results of fluid flow rates. Table 6-4 provide result summaries of CFD simulations for different turbulent models with high pressure boundary condition which are graphically illustrated in Chart 6-1. Sufficient grid quality was evaluated based on percentage deviation of following mass flow leakage results using increasing grid quality.

Table 6-4 Results of mass flow leakage for High pressure boundary conditions

Mesh		**Mass flow rate [kg/s]**		
Mesh Type No.	Number of nodes	Standard k-ε	SST k-ω	Reynolds stress
1	3 556	2,1326	1,9794	2,1663
2	7 382	2,1326	1,7901	1,9660
3	25 552	2,1174	1,7870	1,8436
4	37 965	2,0686	1,7747	1,8166
5	79 149	2,0302	1,7170	1,7877
6	99 521	2,0279	1,7158	1,7810
7	165 526	2,0234	1,7154	1,7800
8	496 571	2,0256	1,7247	1,7850

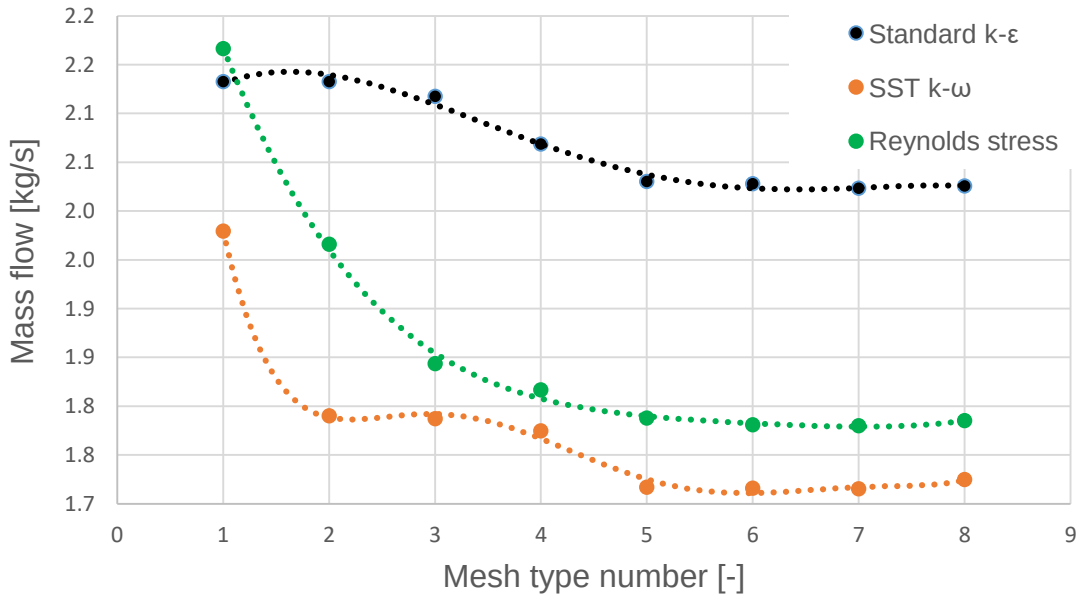

Figure 6-3 Grid independence analysis of mass flow leakage for high pressure boundary conditions

The Figures 6-3 to 6-5 shows the contours of velocity magnitude and static pressure (see *Appendix B*) across the whole labyrinth seal and describes the increase of kinetic energy of fluid flow through teeth and stator clearance by throttling and converting pressure difference energy to kinetic energy.

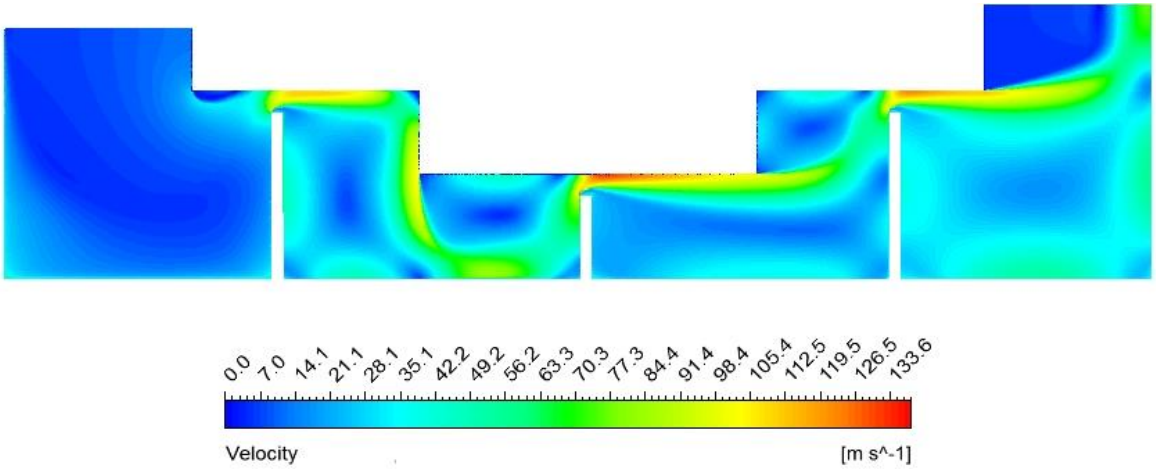

Figure 6-4 Velocity magnitude of fluid using k-ε model

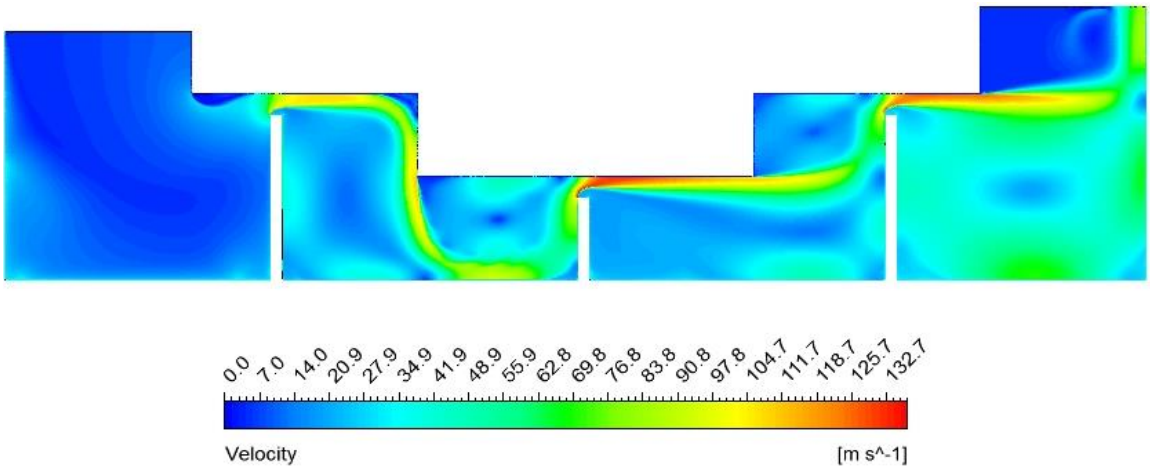

Figure 6-5 Velocity magnitude of fluid using Reynolds stress model

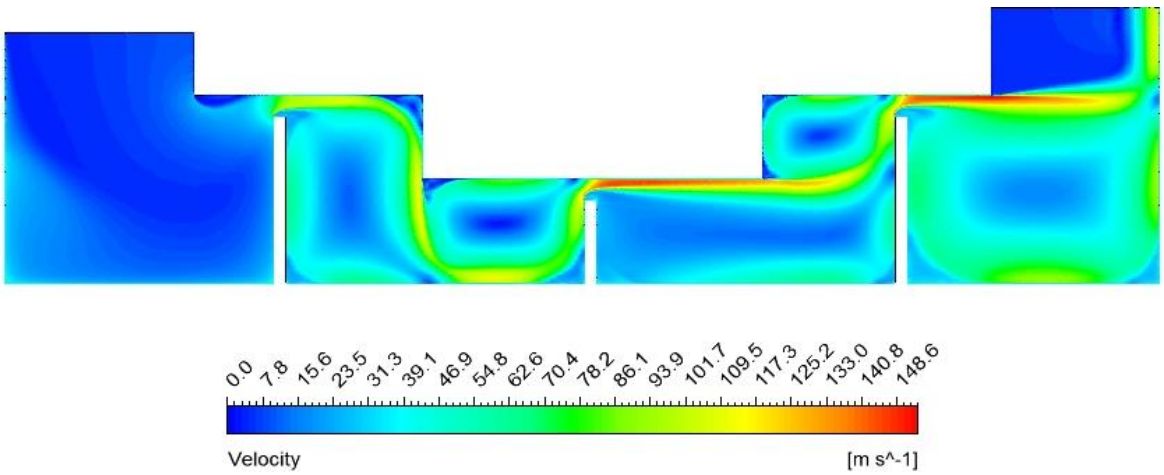

Figure 6-6 Velocity magnitude of fluid using SST k-ω model

The stream function plots (see Figures 6-6 to 6-8) show several areas of recirculating flow. The flow recirculation patterns are consistent applying different turbulent models, however resulting in various ranges. The areas with higher recirculating vortices exist upstream before fluid is entering second and third tooth-stator clearance of labyrinth seal, where most of the kinetic energy associated with the flow is dissipated. The low recirculating stream locations, are as was expected after the throttling of fluid in the cavity, where the fluid is accelerated by converting static pressure. After each throttle some of the kinetic energy associated with the flow is dissipated by turbulence induced by the intense shear stress and eddy motion in the next chamber. As we can see from the mass flow rates results (Table 6-4) and (Figures 6-6 to 6-8), when more mass flow is concentrated in high recirculating vortices, more kinetic energy is dissipated in the cavity and therefore less of the mass flow leaks through the labyrinth seal.

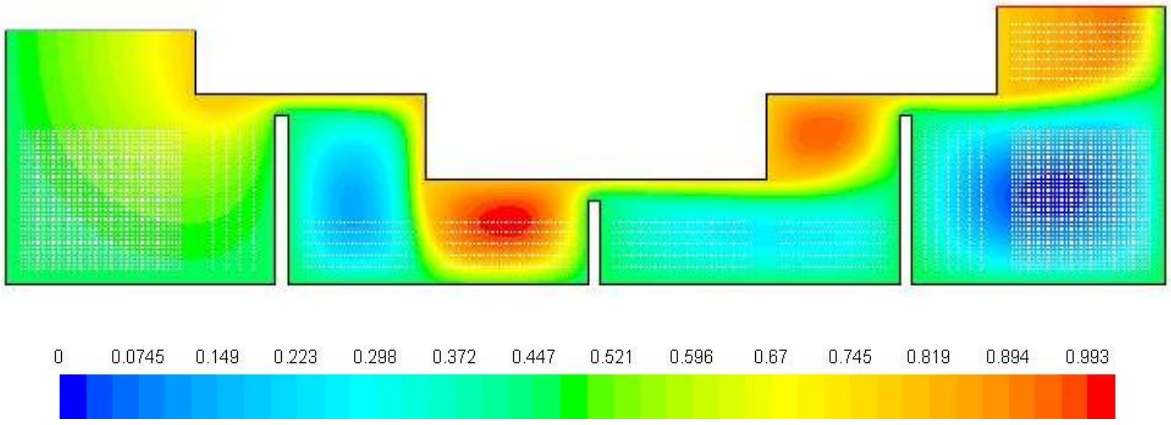

Figure 6-7 Stream function [kg/s] of fluid using k-ε model

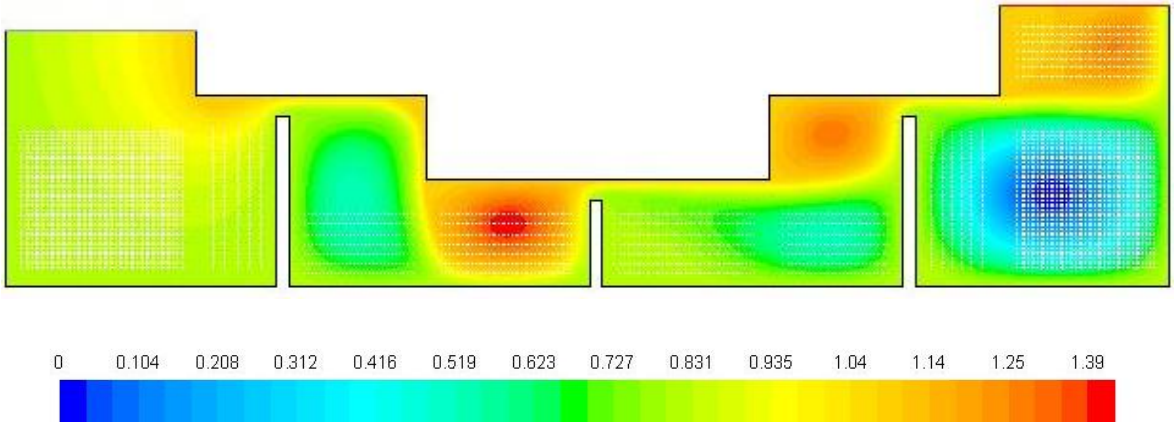

Figure 6-8 Stream function [kg/s] of fluid using Reynolds stress model

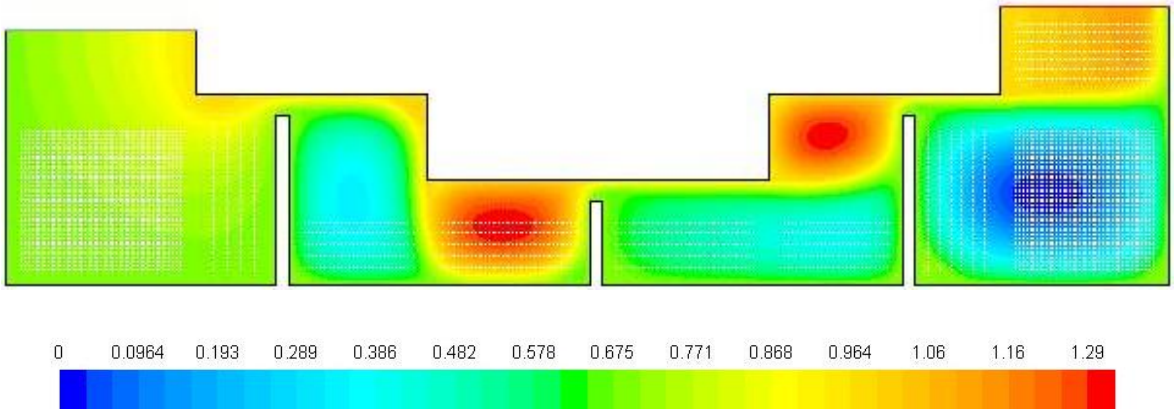

Figure 6-9 Stream function [kg/s] of fluid using SST k-ω model

The numerical data (see Table 6-4 and Chart 6-1) proves that mass flow rate results of all three turbulent models are steady using mesh type number 5, 6, 7 and 8, when the maximum deviation between mass flow leakage rates is 0,54%. Therefore as a sufficient mesh type number 6 (see Table 6-2; $a_0=5\cdot10^{-4}$ mm and q=1,2) is chosen and applied for following simulations using wide range of pressure ratios. The comparison of analytical data and computed results indicates that the most suitable turbulent model possible to use out of three tested is Standard k-ε turbulent model. However even the results using Standard k-ε turbulent model match the analytical data with minimal deviation of -21,8 % (see Table 6-7). The Samoylovich's and Kearton's leakage models correlate with the numerical data the most, on the other hand Zalf formula rapidly overestimates the mass flow prediction.

Table 6-5 Numerical and analytical data of mass flow leakage for high pressure boundary condition

ANALYTICAL RESULTS	
Parameters	Mass flow rate [kg/s]
Samoylovich	2,469573
Stodola	2,510343
Aungier	2,635235
Kearton	2,484177
Zalf	3,502346

ANALYTICAL RESULTS	
Turbulent models	Mass flow rate [kg/s]
STANDARD k-ε	2,027874
SST k-ω	1,715820
Reynolds stress	1,780955

Table 6-6 Deviation between numerical and analytical data for high pressure boundary condition

Parameters	Deviation between numerical and analytical data [%]				
	Samoylovich	Stodola	Aungier	Kearton	Zalf
STANDARD k-ε	-21,8	-23,8	-30,0	-22,5	-72,7
SST k-ω	-43,9	-46,3	-53,6	-44,8	-104,1
Reynolds stress	-38,7	-41,0	-48,0	-39,5	-96,7

The most steady results of mass flow rates (see Chart 6-1, Table 6-4) predicted applying increasing grid resolution was achieved by Standard k-ε turbulent model, where last four predictions of mass flow rates using mesh types 5,6,7 and 8 (see Table 6-2 and *Appendix A*) were in range varying by maximum 0,22 %. It needs to be said that using k-ε turbulent model results in higher mass flow rate than using SST k-ω model or Reynolds stress model. Morrison and Al-Ghasem [11] showed to accurately resolve viscous sub layer without additional effort in terms of more refined mesh Standard k-ε model with enhanced wall function in the near wall region can be applied, placing nodes closest to the walls, in order to get values Y^+ less than 10. In this project even the highest resolution of the grid using $a_0=10^{-4}$ mm was not able to provide Y^+ less than 10 across the whole labyrinth seal. Therefore the scalable wall function was accomodated to the CFD simulations. However it confirms that the most suitable turbulent model for predicting mass flow leakage out of three tested is Standard k-ε model. [4],[16]

7 RESULTS AND DISCUSSION

The stepped, labyrinth seal with 0,5 mm radial clearance is used for numerical and analytical evaluation. The primary concern of this study is to determine the leakage rate through the seal and how it varies with operating conditions, such as different pressure ratios and inlet boundary conditions mentioned in Table 7-1. The settings of CFD simulation with shaft rotation at 3000 rpm and Standard k-ε model which was selected as a turbulent model predicting the mass flow leakage in comparison with analytical data the most are described in previous sections. The default constant values for the model inside FLUENT were used.

Table 7-1 Inlet boundary conditions

Boundary conditions	Pressure [MPa]	Temperature [K]
High pressure	`17,80	847,10
Intermedial pressure	3,40	853,15
Low pressure	0,35	556,15

Figures 7-1, 7-2 ,7-3 and data in *Appendix C* compares the leakage mass flow rates for different boundary conditions obtained from both analytical and numerical simulations. The charts and results of mass flow rates calculated by empirical formulas, we can notice the shape of each graph is exactly the same for all three inlet boundary conditions. After numerical check it has been proven that the deviation between all formulas at the same pressure ratio is constant. Therefore the inlet boundary conditions do not affect the slope of each graph, but they definitely affect the resulting value of mass flow leakage through the seal. The graphs of mass flow rate show similar trends: first a significant growth at high pressure ratios, then it slows down and in three cases (Kearton, Samoylovich and Zalf) it is even levelling out with eventual decline at low pressure ratio.

The inlet boundary conditions in this work are used in real installation of HP, IP and LP steam turbines at the inlet to the first stage. The pressure ratios (0,94 ;0,9 ;0,8) labelled by red colour in tables of Appendix C were found at the instruction book for each turbine and thus we will take a closer look on prediction of mass flow leakage at pressure ratios from 0,7 to 0,94, where even small change of pressure difference has high impact on the mass flow rate. At high pressure ratio the lowest mas flow rate prediction out of five tested leakage models gives the Samoylovich formula. However the Kearton equation results in even smaller values than Samoylovich at pressure ratios below 0,85. The same characteristic is when Stodola and Eungier empirical formula is used, but it results in higher mass flow rates. The results by Stodola equation is closer to the Samoylovich and Kearton at higher pressure ratios and it grows with increasing pressure difference. The opposite effect has the Eungier equation. The maximum deviation of four mentioned leakage models is 6,71 % at same operating conditions. The accuracy between Samoylovich and Kearton mass flow prediction are in the range from 0,59 % to -1,25 %. The Zalf formula seems to be too conservative since it has on average 41% higher results than Samoylovich and Kearton equation.

The CFD prediction of mass flow rate is strongly dependent on parameters of the steam at the inlet. It is obvious from the graphs that for high inlet pressure the resulting value is below the analytical calculations. However when the inlet pressure decreases the CFD prediction grows in comparison with existing leakage models. When high and intermedial pressure boundary conditions are applied, the numerical results match the analytical data calculated by Samoylovich and Kearton the most. Although overall results by Kearton equation are more accurate in comparison with numerical data than others, the approach by Samoylovich is preferable to use at high pressure ratios, where the labyrinth seal are usually designed to operate. The mass flow prediction by Stodola empirical formula was the most suitable for low pressure boundary conditions.

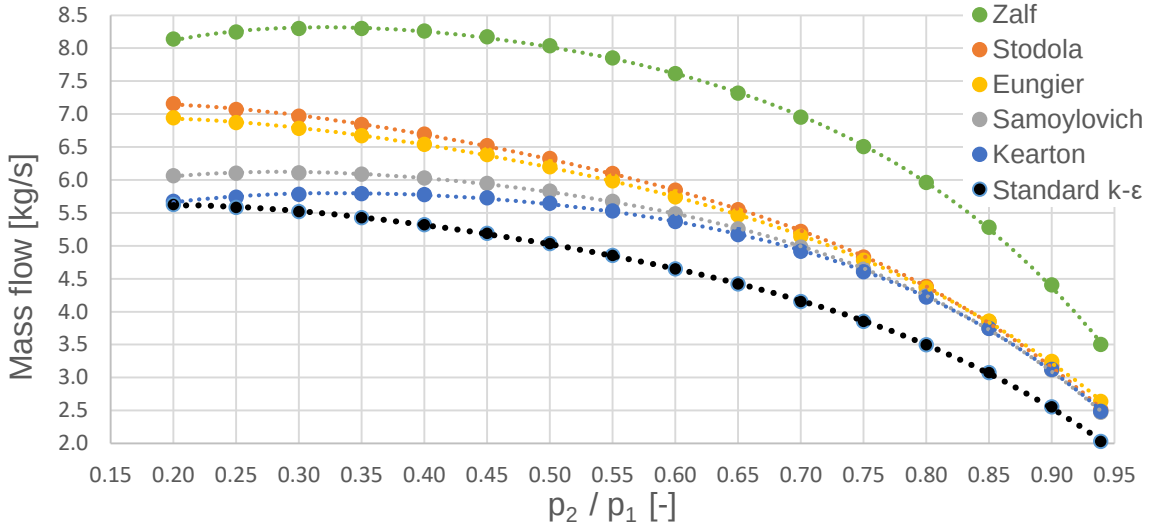

Figure 7-1 Mass flow rates at high pressure boundary conditions

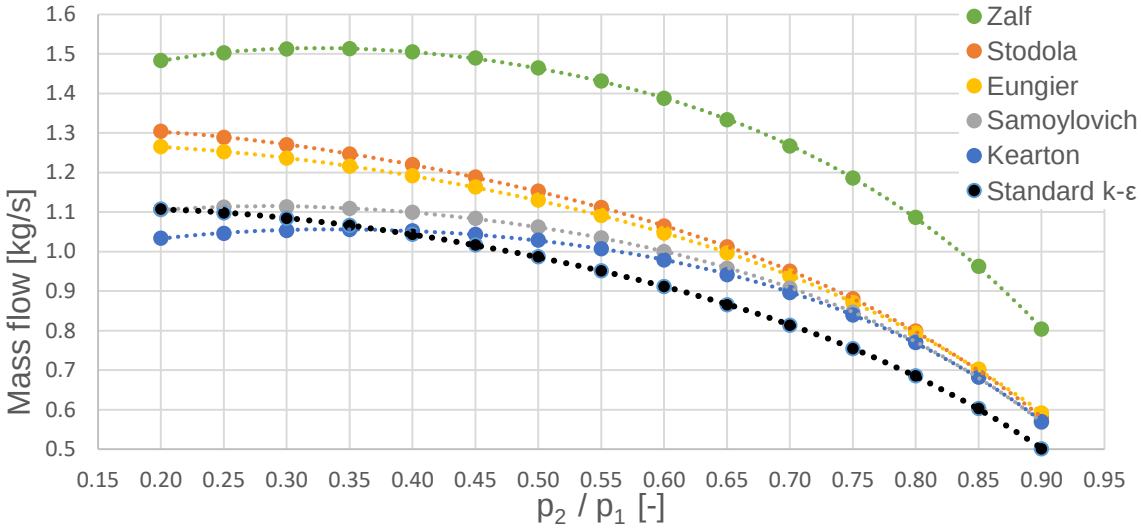

Figure 7-2 Mass flow rates at intermedial pressure boundary conditions

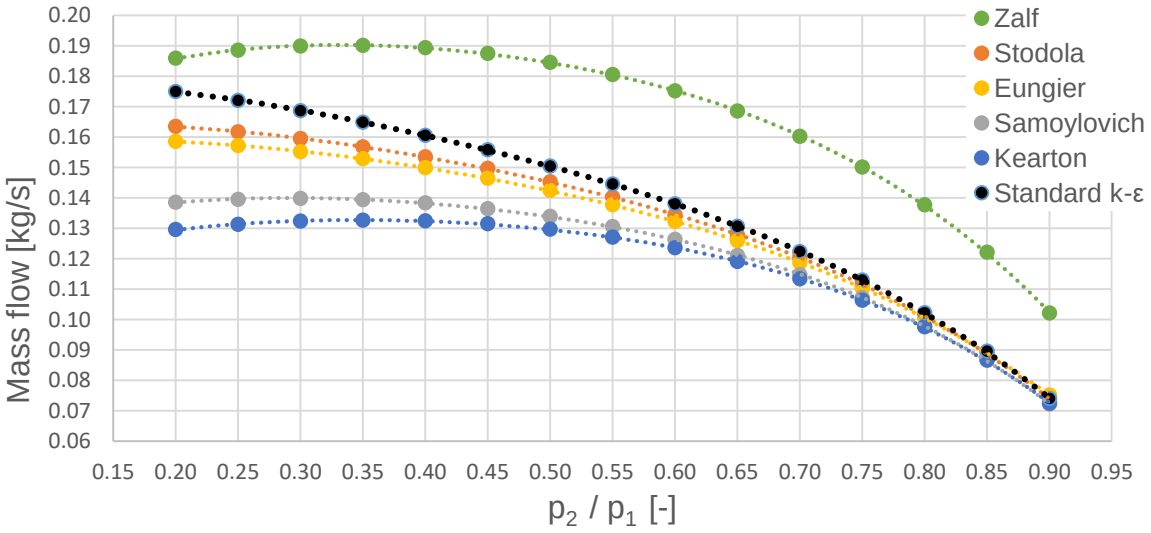

Figure 7-3 Mass flow rates at low pressure boundary conditions

8 CONCLUSION

The primary concern of this study is to determine the leakage rate through the seal and how it varies with operating conditions. Stepped, labyrinth seal with three teeth and 0,5 mm radial clearance is used for both, numerical and analytical evaluation. The results are compared in order to find suitable turbulent model for CFD simulation. The Standard k-ε, SST k-ω and Reynolds stress turbulent model were implemented to the study. A 2D axisymmetric model using scalable wall function with values Y+ less than 30 computed steady results, when all three turbulent models were applied. Comparison of the empirical and numerical results confirmed that the most suitable turbulent model is Standard k-ε, which has been proven by Morrison and Al-Ghasem [11].

The analytical prediction of mass flow rates are always in order, when different boundary conditions are applied. The empirical formula by Kearton, Samoylovich, Eungier, Stodola and Zalf are sorted from lowest to highest results. However the Kearton equation gives higher mass flow rates than Samoylovich at pressure ratios over 0,85. At high pressure boundary conditions the analytical approach overestimates the results comparing to CFD simulations using Standard k-ε model. On the other hand when the inlet pressure decreases the values of numerical results rises above all analytical predictions except Zalf formula. Therefore we can say that the state of the art (Zalf) is too conservatice for predicting mass flow leakage through the stepped labyrinth seal.

For high and intermedial pressure boundary conditions (Table 7-1) the data in *Appendix C* shows the best relation with numerical results given by the Kearton's formula. However most of the labyrinth seals operates at high pressure ratios, where the Samoylovich equation meets the CFD results with higher accuracy than Kearton. The Stodola equation matched the data with average percentage deviation of 3,2 %, when low pressure boundary conditions were applied. Therefore is the best for predicting mass flow leakage using inlet pressures below 0,35 MPa.

9 REFERENCES

[1] GAURAV CHAUDHARY. *LABYRINTH SEAL LEAKAGE ANALYSIS*. USA, 2011. Thesis. Texas A&M University

[2] AHMED MOHAMED GAMAL ELDIN. *LEAKAGE AND ROTORDYNAMIC EFFECTS OF POCKET DAMPER SEALS AND SEE-THROUGH LABYRINTH SEALS*. USA, 2007. Dissertation. Texas A&M University

[3] CHILDS, PETER R.N.. (2014). *Mechanical Design Engineering Handbook - 14.2.2 Gaskets*. (pp. 2-20). Elsevier. Online version available at: http://app.knovel.com/hotlink/pdf/id:kt00C7BZK1/mechanical-design-engineering/gaskets

[4] SAIKISHAN SURYANARAYANAN. *LABYRINTH SEAL LEAKAGE EQUATION*. USA, 2009. Thesis. Texas A&M University.

[5] ŠKOPEK, JAN. *Tepelné turbíny a turbokompresory*. 1. vyd. Plzeň: Západočeská univerzita v Plzni, 2010, 244 s. ISBN 978-80-7043-862-6.

[6] AUNGIER, RONALD H. *Turbine aerodynamics: axial-flow and radial-inflow turbine design and analysis*. New York: ASME Press, 2006, xv, 394 p. ISBN 9780791802410.

[7] ŠČEGLJAJEV, ANDREJ VLADIMIROVIČ. *Parní turbíny: Teorie tepelného děje a konstrukce turbín*. První. Praha: Nakladatelství technické literatury, 1983, 368 s.

[8] ŠČEGLJAJEV, ANDREJ VLADIMIROVIČ. *Parní turbíny: Teorie tepelného děje a konstrukce turbín*. První. Praha: Nakladatelství technické literatury, 1983,

369-630 s.

[9] NING LI. *COMPARISON BETWEEN THREE DIFFERENT CFD SOFTWARE AND NUMERICAL SIMULATION OF AN AMBULANCE HALL* [online]. STOCKHOLM, 2015 [cit. 2016-08-22]. Online version available at: http://www.diva-portal.org/smash/get/diva2:792705/FULLTEXT01.pdf. Thesis. KTH School of Industrial Engineering and Management. Supervisor Joachim Claesson.

[10] INAM, ORCUN. *LABYRINTH SEAL LEAKAGE ANALYSIS* [online]. USA, 2011 [cit. 2016-08-22]. Online version available at: http://oaktrust.library.tamu.edu/bitstream/handle/1969.1/ETD-TAMU-2011-08-10060/INAM-THESIS.pdf?sequence=2. Thesis. Texas A&M University. Supervisor Jerald A. Caton.

[11] MORRISON, G.L. AND AL-GHASEM,A., 2007, "Experimental and Computational Analysis of a Gas Compressor Windback Seal," GT2007-27986, *Proceedings of ASME Turbo Expo 2007*, Montreal, Canada, May 14-17.

[12] JOHNSON M.C., 1989, "Development of a 3-D Laser Doppler Anemometry System with Measurements in Annular and Labyrinth Seals," Ph.D. dissertation. Texas A&M University, College Station

[13] NAVIER-STOKES EQUATIONS. *COMSOL* [online]. North America, 2016 [cit. 2016-09-05]. Online version available at: http://www.comsol.com/multiphysics/navier-stokes-equations

[14] FLUID DYNAMICS: The Navier-Stokes Equations. In: *Andrew Gibiansky* [online]. 2011 [cit. 2016-09-05]. Online version available at: http://andrew.gibiansky.com/downloads/pdf/Fluid%20Dynamics:%20The%Navier-Stokes%20Equations.pdf

[15] ANSYS FLUENT THEORY GUIDE: Release 15.0 [online]. Canonsburg, 2013 [cit. 2016-09-05]. Online version available at: http://148.204.81.206/Ansys/150/ANSYS%20Fluent%20Theory%20Guide.pdf

[16] PAUL HIESTER. *Computational Fluid Dynamic Simulation of a Straight Labyrinth Seal* [online]. Connecticut, 2013 [cit. 2016-09-10]. Online version available at: http://www.ewp.rpi.edu/hartford/~ernesto/SPR/Hiester-FinalReport.pdf. Rensselaer Polytechnic Institute Hartford.Hiester

[17] CHACÓN REBOLLO, TOMÁS A ROGER LEWANDOWSKI. *Mathematical and numerical foundations of turbulence models and applications*. New York: Birkhauser, 2014. Modeling and simulation in science, engineering & technology. ISBN 149390454X.

[18] HASNEDL, DAN, PREMYSL EPIKARIDIS A VACLAV SLAMA. *Experimental Fluid Mechanics 2016: Correction coefficient for see-through labyrinth seal*. Plzen: Doosan Skoda Power, 2016, , 241-244.

10 LIST OF APPENDICES

Appendix A: Additional mesh information i
Appendix B: Static pressure of each turbulent model ii
Appendix C: Mass flow rate results iii